Enabling Near-Zero Emissions and Superior Efficiency in Large-Bore, Medium-Speed Engines with a Hydrogen-Argon Power Cycle

Author(s): Ahammed, Sajid; Ahmad, Zeeshan; Mahmoudzadeh Andwari, Amin; Kakoee, Alireza; Hyvonen, Jari; Mikulski, Maciej

Title: Enabling Near-Zero Emissions and Superior Efficiency in Large-Bore, Medium-Speed Engines with a Hydrogen-Argon Power Cycle

Year: 2025

Version: Accepted manuscript

Please cite the original version:

Ahammed, S., Ahmad, Z., Mahmoudzadeh Andwari, A., Kakoee, A., Hyvonen, J., & Mikulski, M. (2025). Enabling Near-Zero Emissions and Superior Efficiency in Large-Bore, Medium-Speed Engines with a Hydrogen-Argon Power Cycle. *SAE Technical Paper*. 17th International Conference on Engines and Vehicles. SAE International. https://doi.org/10.4271/2025-24-0001

Enabling near-zero emissions and superior efficiency in large-bore, medium-speed engines with a hydrogen-argon power cycle

Abstract

Combustion engines operating on a hydrogen-argon power cycle (H-APC) offer potential for superior thermal efficiency with true zero exhaust emissions. The high specific heat ratio of argon allows extrapolation of the theoretical efficiency of the Otto cycle to almost 90%. However, this potential is significantly constrained by challenges in combustion control, excessive thermal loading, and system integration, particularly regarding argon recovery. This study investigates these trade-offs, within the context of real-world engine-based peaking power plants. An experimentally validated 1D-simulation model of a prototype Wärtsilä 20 DF engine serves as reference for analysis of a retrofit incorporating a closed-loop argon cycle, with dedicated H_2 and O_2 injectors, a water condenser and water separator. Engine performance is evaluated at reference operating point of 75% load, considering pre-ignition, peak pressure and exhaust temperature constraints, condenser limitations, and impurity accumulation. Argon emerges as the best monoatomic gas for H-APC. Helium, the second-best candidate, offers superior thermal conductivity and specific heat, but its low density and molecular weight reduce power output. A 90% argon and 10% oxygen mixture offers the optimal trade-off between power output, efficiency, and durability. A compression ratio of 11.90:1 ensures stable combustion within design constraints, while stoichiometric operation and condenser inlet pressure of 3.23 bar enhances performance, achieving the best indicated gross efficiency of 59.10%. This is over 10 percentage points better than the reference engine at 75% load. Nevertheless, practical implementation is limited by pumping losses in a packaging-optimized argon-path layout, reducing extractable efficiency to 56.70%. Furthermore, just 2% impurities in fuel/oxidizer stream causes progressive efficiency decline, falling below the reference threshold after approximately 10 minutes of operation. This highlights the necessity of a membrane-based separator and system volume optimization. The findings establish a validated computational framework for optimizing closed-loop hydrogen combustion and provide valuable insights for progressing demonstrator development.

1. Introduction

Despite decarbonization efforts, fossil fuels currently supply 80% of global energy. Renewables are projected to account for only 25–28% by 2050, far below the two-thirds threshold recommended by the International Renewable Energy Agency (IRENA) [1], [2], [3].

Transition to renewables for energy generation is hindered by the need to provide fast response to balance the grid, with medium-speed gas engines as state-of-the-art solutions [4]. While their overall efficiency in combined heat and power can reach up to 97% [5], there are limited possibilities to valorize excess heat. Hence, maximizing thermodynamic efficiency and accommodating zero-carbon fuels are key objectives for these engine generators.

While combustion engines are gaining ground as a solution to cover deficits of wind and solar, the excess energy from these renewable sources needs to be captured by energy storage systems (ESS). Storing energy in the form of hydrogen (H_2) is regarded as a future solution for the circular economy [6]. However, the concept has not moved beyond the technology readiness level of 7/10 [7]. The circularity aspect remains questionable: electrolysis relies on access to an abundance of clean water, while the business case for selling and transporting green hydrogen is economically challenging [8]. To this end, utilizing H_2 in the argon power cycle (APC) can satisfy the development targets for peaking plants while simultaneously valorizing all products coming from the electrolyzer. A combined peaking-ESS plant can generate H_2 and O_2 when there is excess renewable energy in the grid, taking advantage of a negative electricity price. During the energy deficit period, H_2 and O_2 can be combusted under an argon atmosphere, offering unprecedented efficiency with full recovery of water from the combustion products.

APC offers a high-efficiency alternative to conventional combustion concepts by utilizing argon, a monoatomic gas with a higher specific heat ratio ($\gamma = 1.67$), as working fluid in a closed-loop system. This design eliminates gas loss and enhances thermodynamic performance, surpassing lean-burn gas engines ($\gamma = 1.4$, and ~50% adiabatic efficiency) [9]. The theoretical efficiency of the Otto cycle, governed by Carnot efficiency and Poisson relations, demonstrates that at an identical compression ratio (12.3:1), argon yields significantly higher final temperature (1611.97 K) and pressure (66.09 bar) than air. Consequently, theoretical efficiency increased from 63.4% (air) to 81.4% (argon). This improvement in efficiency necessitated a higher injected mass of argon compared to air [10]. However, challenges such as pre-ignition and thermal stress must be addressed to ensure practical viability [11]. These findings highlight argon's potential as a working fluid for next-generation, high-efficiency combustion engines.

It is worth noting that excessive temperatures necessitate precise combustion control [12], while increased pressure accelerates material degradation, requiring high-temperature-resistant components [13]. Practical implementation demands that these issues are addressed through optimized compression ratios, spark-assisted ignition, and advanced thermal management. [14]. Using an argon-fuel-oxidizer mixture, thermal efficiency can be enhanced by 15–22%, with the theoretical efficiency of the APC reaching up to 90%. Additionally, for instance, in the W20 large-bore, medium-speed engine at a compression ratio (CR) of 12.3:1, the cycle achieved an efficiency of 81.40%, showcasing superior thermodynamic performance in the recent research [10].

Other works, such as small-scale argon cycle experiments by U.C. Berkeley [14], [15] and Toyota [16] and previous analyses of argon's thermodynamic advantages, have stated that APC is particularly effective in small-scale operations using closed-loop argon recycling. Additionally, the injection of hydrogen and oxygen in the H-APC presents significant challenges, including premature combustion, poor mixing, and technical constraints. All these influence pressure, temperature, heat loss, and combustion efficiency [17]. Recent research underscores the necessity of optimizing fuel injection strategies to improve combustion stability, enhance efficiency, and extend the lean limit [18].

A significant study conducted by U.C. Berkeley and Okayama University reported a higher efficiency gain using argon in natural gas

engines [14]. Specifically, the thermal efficiency of 41.5% extended the lean-burn limit, and reduces both oxides of nitrogen (NOx) and unburned hydrocarbon emissions compared to conventional air cycles. Engine load can be effectively controlled through adjustments to equivalence ratio and oxygen content. Furthermore, integration of spark-assisted compression ignition (SACI) further improves efficiency and reduction of emissions. By optimizing both oxygen content and equivalence ratio, along with SACI, the argon power cycle demonstrates efficiency gains that exceed even the reported 15–22% improvement.

A recent SAE paper by Kim et al. [11] examined pre-chamber combustion in an APC engine, specifically focusing on natural gas combustion within an oxygen-argon mixture. Unlike studies on direct H_2/O_2 injection in closed-loop systems, this research emphasizes pre-chamber ignition. This enhances combustion efficiency in highly diluted mixtures, addressing low-load operational challenges. The authors employed a 3D computational fluid dynamics (CFD) model, validated against experimental data, to simulate key combustion parameters, including cylinder pressure and heat release. Their findings demonstrate that argon-breathing engines achieve higher indicated thermal efficiency than air-breathing counterparts. Furthermore, the study investigated the impact of oxidizer composition on performance, highlighting the unique challenges of scaling combustion processes to larger engines. This research contributes valuable insights for optimizing performance in zero-emission combined heat and power (CHP) systems, addressing key modeling issues such as heat transfer during turbulent jet-wall interactions in APC engines.

The impact of CR and mixture composition on H-APC efficiency has been extensively studied, revealing both significant gains and operational challenges. Killingsworth et al. [15] investigated the effect of compression ratio and specific heat ratio on engine efficiency, using a single-cylinder, port fuel-injected, variable-compression ratio Cooperative Fuel Research (CFR) engine. The engine had a displacement of 0.616 L, bore of 82.5 mm, stroke of 114 mm, and a compression ratio range of 4.5:1 to 17:1. Its operating speed was 900 rpm. The experiments, conducted with hydrogen–air and hydrogen–oxygen–argon mixtures, showed that a compression ratio of 5.5:1 produced the highest efficiency for H_2– O_2–Ar mixtures, achieving a peak net indicated thermal efficiency of 44.1% at 86% argon mole fraction. In contrast, H_2–air mixtures at an equivalence ratio of 0.24 reached a peak efficiency of 35.9% at a compression ratio of 13:1. Spark timing for H_2– O_2–Ar was knock-limited above a compression ratio of 4.5:1, while H_2–air operation was not constrained by knock. A three-zone model attributed the higher efficiency of H_2– O_2–Ar to reduced unburned mass in crevices, lower wall heat transfer, and faster combustion from elevated in-cylinder temperatures. Efficiency increased with compression ratio but peaked at 13:1 before declining for both mixtures.

Sierra Aznar´s study [19] examined the use of argon in reciprocating internal combustion engines (RICEs), demonstrating an improvement of up to 30% in thermodynamic efficiency over air-breathing engines. The experimental engine featured a 611cc displacement, a compression ratio of 4:1 to 17:1, a speed range of 300–1200 rpm, an 82.5 mm bore, a 114.3 mm stroke, and a 254 mm-long connecting rod. Key modifications included adjustments to the compression ratio, fuel injection system, and combustion chamber design. Argon's higher specific heat capacity reduced gas temperatures during expansion, minimizing heat losses. Stable operation with port-injected methane was achieved at compression ratios of up to 10:1, compared to 16:1 for air, while hydrogen was limited to a CR below 7:1, due to knocking. Combustion duration decreased, with the highest efficiency at 10% oxygen. Direct fuel injection improved hydrogen combustion but reduced methane efficiency due to the Joule-Thompson effect, highlighting the need for optimized injection strategies.

Wang et al. [9] investigated the APC with the Miller cycle, analyzing how compression ratio, expansion-compression ratio, and argon concentration affect thermal efficiency and power density. Increasing these parameters enhances energy conversion by improving the transformation of sensible internal energy into work. The Miller cycle achieved 70% and 96% of its improvement potential at expansion-compression ratios of 1.5:1 and 2.0:1 respectively. Efficiency gains were greater in Ar-O_2 than N_2-O_2 mixtures, with thermal efficiencies increasing by 7.2% and 6.2%, respectively, when the expansion-compression ratio increased from 1.0:1 to 1.5:1. The Otto cycle required a compression ratio of 9:1 and an Ar concentration of 95% to achieve 70% efficiency, whereas the Miller cycle required only 7:1 and 91%, respectively. Reducing the Ar concentration from 95% to 91% increased power density by 66%. At an Ar concentration of 91% and an expansion-compression ratio of 1.5, indicated thermal efficiencies for compression ratios of 7:1, 11:1, 15:1, and 19:1 were 53.8%, 58.6%, 61.2%, and 62.9%, respectively, with power density gains of 10.7%, 7.5%, 6.0%, and 5.1% over the Otto cycle. Experimental validation is required, focusing on compression ratios of 7:1–11:1, an expansion-compression ratio of 1.5:1, and an Ar concentration of 91%. Advanced ultra-lean combustion and intake pressure boosting are recommended to suppress knock and further enhance efficiency.

De Boer and Hulet [19] studied a single-cylinder ASTM-CFR engine operating on hydrogen, oxygen, and argon mixtures. Thermal efficiency ranged from 30% at low argon concentrations to 50% at high concentrations. Knock issues at high compression ratios limited ignition timing, reducing efficiency. The optimal CR was between 6:1 and 7:1. At argon concentrations above 75%, the engine outperformed hydrogen-air engines in terms of efficiency. IMEP values ranged from 0.37 to 0.65 MPa and were largely unaffected by diluent concentration, unlike H_2/air engines. Thermal efficiency was lower than theoretical predictions due to the knock. Direct fuel injection, which mitigates knock and pre-ignition, could improve performance, though this was beyond the study's scope.

Dibble et al. [20] demonstrated in a patent that a closed-loop argon recycling system with variable valve timing (VVT) optimizes combustion and reduces pre-ignition. The valve timing schemes, tailored for the closed-loop recirculating system and designed for high overall efficiency, focus on controlling intake valve closure. This closure governs the pressure ratio and maximum temperature of the working fluid. Adjusting intake valve closure allows the compression ratio to be reduced, while maintaining a fixed expansion stroke ratio, thus effectively controlling load and ignition timing. Additionally, Sierra Aznar [21] achieved 44% efficiency at 7.3 bar IMEP on NG/O_2/Ar mixtures with direct injection of H_2. Argon-enhanced H-APC cycles can exceed 70% efficiency, but challenges such as knocking and pre-ignition persist, requiring advanced engine designs and combustion control for further optimization.

Previous research on the APC has been confined to small-scale, single-cylinder engines (<1L displacement), optimizing CR, fuel injection, and ignition strategies to reduce knock and thermal stress. Despite these efforts, efficiency gains remain below theoretical predictions due to combustion instability, heat transfer losses, and hardware limitations. The highest reported efficiency of 44.1% at 86% argon mole fraction is a modest improvement on lean-burn natural gas engines (~41.5%) but fall short of the expected 60% threshold.

Large-bore, medium-speed engines must be investigated to exploit APC's full potential. Their ultra-heavy-duty design offers higher tolerances for the mechanical and thermal loading factors critical in practical implementation of high heat capacity cycles. Larger system volumes allow more efficient water-condensers and provide more tolerance for accumulation of impurities. Finally, significantly higher profitability per unit of such engines allows implementation of sophisticated thermal management and pre-ignition avoidance strategies, including variable valve actuation or high-pressure gas-phase direct injection. Such technologies were unattainable for earlier studies based on low-cost, light-duty designs. This study, for the first time, investigates the feasibility of the hydrogen-argon cycle in the context of its intended application in high power density peaking power plants. An experimentally validated 1D-simulation model of a prototype Wärtsilä 20 DF four-stroke, medium-speed engine serves as the reference for an analysis of a retrofit incorporating a closed-loop argon cycle, with dedicated H_2 and O_2 injectors, a water condenser and a water separator. Engine performance is evaluated at reference operating point of 75% load, considering pre-ignition, peak pressure and exhaust temperature constraints, condenser limitations, and impurity accumulation. The study forms pre-design constraints for the corresponding world-first relevant-scale (150kW/per cylinder) demonstrator of the APC technology to be built in Finland by the iHAPC consortium [22].

2. Materials and methods

2.1 The object and sources for reference experimental data

The geometrical and reference data used for the identification, calibration, and validation of the modeling toolchain in this study are derived from a prototype dual-fuel research engine at Wärtsilä Laboratories in Vaasa, Finland. The Wärtsilä 6L20-2STC (W6L20) engine serves as the reference. Its performance parameters, geometric specifications, and operational characteristics form the foundation for the adaptation of the H-APC in GT-Suite. This engine is a six-cylinder, two-stage turbocharged, dual-fuel Wärtsilä model with a 200-mm bore, widely used in marine and power generation applications. Table 1 lists its key specifications [23]. The engine's performance is analyzed under 50%, 75%, and 100% load conditions.

The W6L20 is a four-stroke, in-line, six-cylinder marine engine designed for diesel-electric propulsion, delivering 1200 kW at 1000 rpm. It features a piston displacement of 8.8 liters per cylinder and a stroke length of 280 mm. The engine incorporates a two-stage turbocharging system and supports dual-fuel operation, utilizing a high-reactivity marine diesel oil (MDO) common-rail fuel system in conjunction with a low-pressure, multipoint methane injection system. Furthermore, the engine has electrohydraulic valve actuation, enabling full variability in valve lift and timing.

The two-stage turbocharging system, arranged in series, includes both low- and high-pressure compressors and turbines, thereby optimizing air intake and exhaust efficiency. Fuel injection is managed by centrally mounted, single-needle injectors, which control the direct injection of high-reactivity pilot fuel and full diesel injection during diesel mode.

Table 1: The specification of the reference Wärtsilä 6L20-2STC engine [23]

Specification	Details
Engine type	four-stroke
Piston displacement	8.8 liters per cylinder
Cylinder bore	200 mm
Stroke	280 mm
Air system	two-stage turbocharged (in series)
High-reactivity fuel system	MDO-Common rail
Low-reactivity fuel system	methane, low-pressure; multipoint, upstream of the intake valve
Valvetrain	four valves per cylinder, fully variable hydraulic valvetrain
Cylinder configuration	inline, six cylinders
Speed	1000 rpm
Mean piston speed	9.3 m/s
Power output	1200 kW (diesel electric propulsion)

A multipoint gas injection system, regulated by a low-pressure solenoid valve, delivers methane upstream of the intake valves. In dual-fuel operation, the W6L20-DF engine employs low-pressure port fuel injection (PFI) of methane at 10 bar (-360° CA) and direct injection (DI) of MDO with variable timing. Intake and exhaust pressures are maintained at 1.01 bar, while boost pressures range from 3.46 to 5.95 bar, depending on the load conditions. It operates at a compression ratio of 12.3:1.

2.2 The simulation framework

2.2.1 1D-model of the reference engine

The GT-Suite W6L20 engine model employs a zero-dimensional combustion approach with map-based turbocharger sub-models, accurately representing the combustion, intake, exhaust, and turbocharging systems provided by Wärtsilä. Each subsystem is modeled using bends, orifices, contractions, intercoolers, and flow splits to simulate engine dynamics with high precision. Overall, the model has 662 individual flow components (pipes and flow splits). A steady-state assumption governs intake and exhaust flows, with manifold pressure and temperature prediction based on engine speed and load. Ambient conditions serve as reference points for evaluating performance at varying loads. To capture dynamic variations in pressure, temperature, velocity, and mechanical forces, the discretization length (exhaust 110mm; intake 80mm) is scaled relative to bore size (200mm), ensuring accuracy in flow modeling.

The turbocharging system, consisting of low- and high-pressure compressors and turbines, is parameterized using experimentally validated maps which define pressure and temperature characteristics. Intercoolers, modeled as heat exchangers, regulate compressed air temperature before combustion. The combustion process is defined by

an imposed burn rate, determined through the three-pressure analysis (TPA) method. Heat transfer is calculated using the Woschni GT model, which assesses cylinder-wall interactions to estimate thermal efficiency. Exhaust temperature is imposed to streamline thermal modeling; while piping wall temperature remains fixed and cylinder wall temperature is derived from empirical data, reflecting real operating conditions. The fuel injection system integrates low-pressure methane port fuel injection (PFI) and MDO direct injection (DI) via the injection profile connection template. A governor injector controller facilitates seamless transitions between dual-fuel and diesel-only operation, optimizing combustion across varying conditions. Valve timing, regulated through the RLT variable creator, ensures synchronized intake and exhaust events, enhancing efficiency.

2.2.2 Establishing the H-APC model, based on reference engine setup

The integration of the H-APC system into the W6L20 engine GT-Suite model requires precise calibration and validation. This process follows a structured approach, beginning with model adaptation and validation (Step-1). Initially, in second step, a validated single-cylinder model was derived from the reference multicylinder dual-fuel engine model. The model was then modified into an open-cycle argon configuration by replacing the working fluid and fuel. This setup was subsequently converted into a closed-loop H-APC system by integrating a controller, substituting air with argon, and incorporating a condenser unit to eliminate the exhaust steam and recirculate the argon back to the closed-loop system in the third step. Finally, the model was scaled to a multi-cylinder configuration through modifications to the controller and fuel injector to accommodate increased system complexity.

The next phase focused on optimizing the controller mechanism for hydrogen and oxygen injections to ensure their precise regulation. This optimization adjusted the boost pressure to achieve the required trapped mass in the cylinders, while maintaining stable energy levels during initial testing. The valve timing from the six-cylinder reference model was retained. Figure 1 provides a detailed overview of each development step and highlights key subsystem modifications.

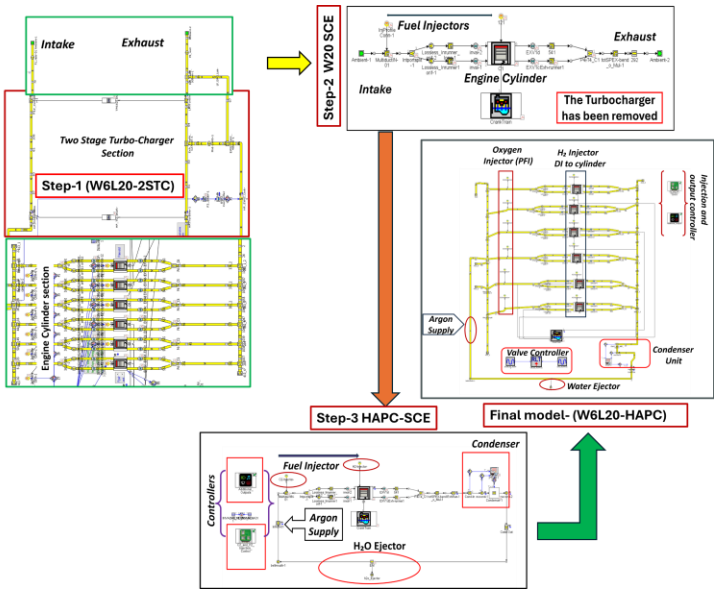

Figure 1: Development of the 1D model for the H-APC, based on the W6L20-2STC reference engine.

The combustion modeling approach remained consistent with the reference engine. User-imposed combustion profiles, derived via the TPA method, and key combustion parameters, such as start of combustion (CA02), crank angle at 50% mass burned (CA50), and burn duration were considered to be the same as for reference engine. This assumes that the optimal combustion progress of hydrogen can be maintained via engine control measures. Particularly with high-pressure direct injection of hydrogen, considered as enabling solution for iHAPC, both the (auto)ignition and combustion onsets can be controlled via the diffusion rate of hydrogen jet. This assumption is further considered beneficial from the perspective of the objective of the present study as it enables to decouple the effects of argon on thermodynamic efficiency from masking effects related to indicated and combustion efficiency, considered practical limits of peak pressure rise rate and peak thermal loading.

The engine model employs the Chen-Flynn friction mean effective pressure (FMEP) model, as detailed in the GT Suite Engine Performance Manual. The cylinder blow-by model simulates the leakage path between the combustion chamber and the crankcase, thus representing real engine behavior. The full engine model must reproduce cylinder pressure analysis results, while accounting for blow-by effects.

Finally, the cylinder heat transfer is modeled using the Woschni GT correlation, calibrated for the reference engine. The lack of global data on heat flux for argon, in typical engine conditions, substantiates this simplification. Note however, that the anticipated effect of elevated heat losses in argon is captured through direct dependency of the Woschni correlation on in-cylinder pressure and temperature (calculated from detail gas properties). Together with mean fluid flow intensity (considered unchanged with the same engine geometry) these are the governing terms influencing the convective heat transfer mechanism. With radiation effects considered negligible, different thermal conductivity of argon compared to air has secondary effect on overall heat transfer rate. Considering the above, the heat loss calculation methodology in the model is considered trend-wise valid for argon. The absolute results should, however, be treated with caution, as the modeling approach further assumes that cylinder wall temperatures can be kept the same as in the reference engine.

The condenser unit was modeled using a semi-predictive heat exchanger approach, guided by an intercooler efficiency template to condense water vapor, a key by-product of the H-APC. The modeling of the condenser, defined by pipe number, diameter, and length, was based on the pressure drop before and after the condenser unit. A water ejector template, similarly, opposite to the injector sub-model, facilitated water ejection. An output controller, utilizing a math equation template, was employed for steam-water separation via the ejector, ensuring proper mass balance. Oxygen and hydrogen injection sub-models were governed by RLT monitor units and mathematical equations, achieving steady-state operation.

2.3 Design of simulations

The GT Suite software was used during the systematic analyses to investigate various research questions, with adjustments made by the fuel injection controller unit within the modeled closed-loop cycle. At 95% condenser effectiveness and a coolant temperature of 345 K, the volumetric efficiency closely matched that of the reference engine. The intake valve closing lambda and exhaust temperature had negligible effects on volumetric efficiency when the condenser effectiveness was set to 90%. Table 2 summarizes the simulation design framework with all parameters.

In the argon/oxygen ratio and optimal O_2-fuel ratio sweeps, hydrogen fuel quantity and oxygen-to-argon ratio in the intake pipe were modified by adjusting mass fractions to maintain constant power output and combustion phasing (e.g. CA50). This methodology effectively isolated the effects of mixture composition and the O_2-fuel ratio. The combustion burn rate remained consistent across all cases, with CA10, CA50, and burn duration unchanged across different load conditions. Pure argon, pure helium, and a 50%-50% argon-helium mixture were tested as working fluids for the alternative monatomic gas analysis. The gas mixture was varied by adjusting the intake pipe configuration. Compression ratios were evaluated between 6:1 and 12.3:1, with a constant fuel injection rate. Exhaust backpressure, defined as the pressure before the condenser, was regulated between 3.23 and 4.25 bar by a pressure control valve to maintain consistent operational conditions. Finally, the impact of hydrogen fuel containing 2% nitrogen impurities (98% hydrogen) on engine performance was analysed. The simulations revealed that these impurities led to a gradual decline in engine efficiency, with a noticeable drop over time.

Table 2: Summary of the simulation design framework

Test case	Sweep description	Parameter sweep	Method	Test conditions		Injected fuel mass	Valve setting	Test fuel / mixture	Objective	Combustion parameters (per load)
Baseline setup	–	–	-	**Speed**	1000 rpm	reference / varies	same as W6L20 model	fuel: H_2 working fluid: Ar, He, Ar+He	define baseline performance conditions	–
				CR	12.3:1					
				Coolant temp	345 K					
				Simulation type	closed-loop, steady-state					
				Combustion model	imposed burn rate (TPA)-W6L20-2STC					
Sweep										
1	Ar-to-O_2 ratio	(90% Ar + 10% O_2) → (80% Ar + 20% O_2)	simulation	load: 50%, 75%, 101%		varies with load and mixture	〃	stoichiometric H_2:O_2 (1:8)	assess combustion behavior under varying dilution ratios	ref. 50% load 75% load 100% load
2	alternative monatomic gases	Ar, He, (Ar+He) [50/50-blend]	simulation	load: 75% mixture: 90% diluent + 10% O_2		300 mg/c	〃	H_2 fuel	compare performance of different working fluids	same as sweep 1 (75% load)
3	λ (O_2-to-fuel ratio)	λ = 0.85, 1.00, 1.20, and 1.40	simulation	load: 75% mixture: 90% Ar + 10% O_2		varies with λ	〃	H_2 fuel	evaluate effect of rich/lean mixtures on combustion	〃
4 (a)	compression ratio	CR range: 6 ⇅ 12.3	simulation	load: 75% mixture: 90% Ar + 10% O_2		300 mg/c	〃	H_2 fuel	investigate impact of CR on performance and efficiency	〃
4 (b)	exhaust back pressure	$P_{int,cond}$ = 3.23, 3.30, 4.00, 4.25 bar	simulation	load: 75% mixture: 90% Ar + 10% O_2		300 mg/c	〃	H_2 fuel	study influence of exhaust pressure before condenser	〃
5	hydrogen fuel impurities	H_2 (98%) + N_2 (2%)	simulation	load: 75% mixture: 90% Ar + 10% O_2 CR = 12.3:1		300 mg/c	〃	H_2 fuel with 2% N_2 impurity	assess performance loss due to impurity	〃

It is important to note that the combustion models integrate a non-predictive method with real-world performance data to accurately simulate the combustion characteristics of the H-APC system for the W6L20 engine. This model facilitates the evaluation of engine performance under constant airpath geometries, different mixture compositions, charge pressures, and fueling conditions, provided that combustion is maintained at its reference point through control mechanisms. However, the non-predictive nature of the model limits its ability to capture the effects of argon ratio and fuel/charge stratification on combustion duration at a given ignition setpoint. This study acknowledges these limitations.

3. Result and discussion

3.1 Model validation and design constraints

3.1.1 Reference engine simulated data

Figure 2 shows the reference engine model simulated over 175 cycles to reach a steady state, with performance evaluated at 50%, 75%, and 100% load to identify key operating points and set design constraints.

At 50% load, the engine operates at a boost pressure of 3.50 bar, injecting 310.85 mg of fuel per cycle. The IMEP and BMEP at this load was recorded 15.77 bar and 13.70 bar, respectively, with indicated and brake efficiencies of 47.89% and 41.95%. The peak in-cylinder pressure and peak temperature at 50% load reach 160.98 bar and 1693.73 K respectively, with a maximum exhaust temperature of 814 K. The lambda values at intake valve closing (IVC) and exhaust valve opening (EVO) are 4.26 and 2.56, respectively, yielding a brake power output of 602.58 kW.

With the load raised to 75%, the boost pressure increases to 4.82 bar, with an injected fuel mass of 441.17 mg per cycle. The IMEP and BMEP raise to 22.73 bar and 20.67 bar, while indicated and brake efficiencies improve to 48.98% and 44.60% respectively. The peak in-cylinder pressure rises to 208.91 bar and peak temperature reaches 1691.89 K, with an exhaust temperature of 833 K. The lambda values decrease to 4.17 at IVC and 2.46 at EVO, and the brake power output reaches 908.59 kW.

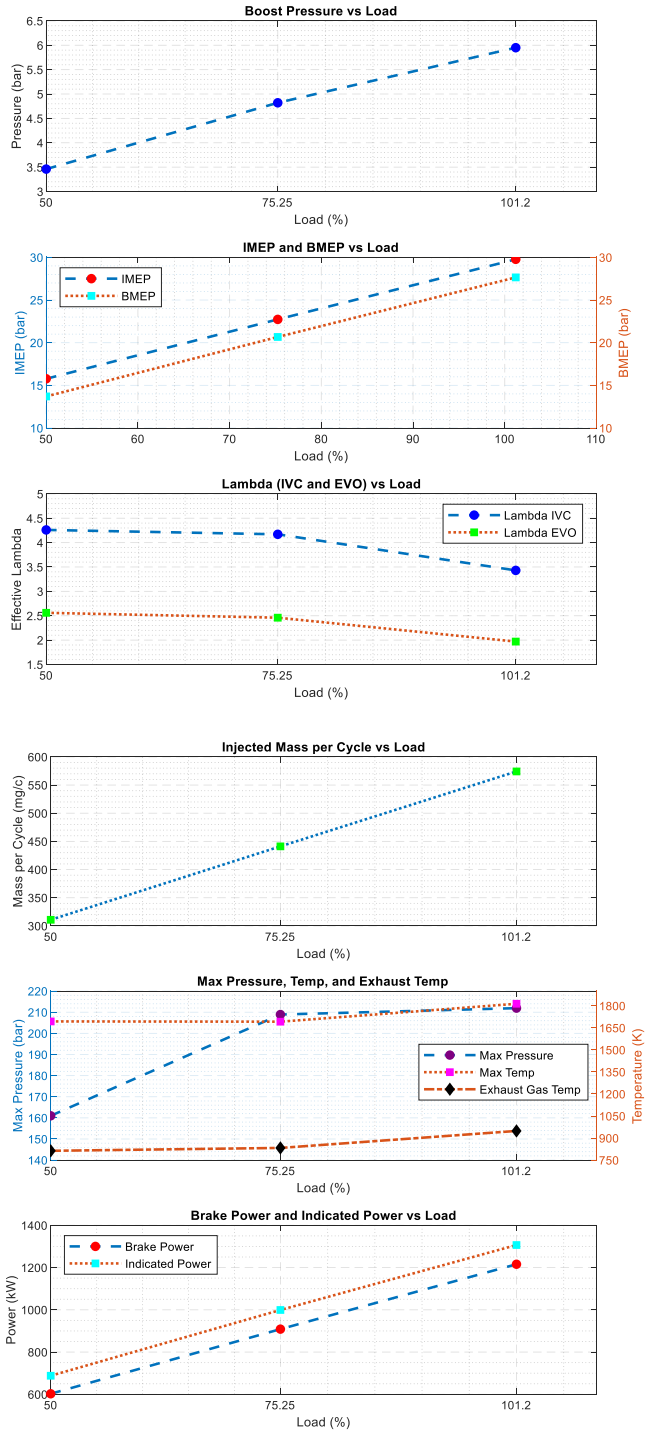

Figure 2: Reference GT Suite simulated data for engine performance measures in the W6L20-2STC model

At full load (100%), the boost pressure reaches 6.00 bar, with an injected fuel mass of 574.14 mg per cycle. The IMEP and BMEP attain 29.77 bar and 27.65 bar, respectively, with indicated and brake efficiencies of 49.21% and 45.82%. The peak in-cylinder pressure rises to 211.93 bar and peak temperature is 1813.91 K, while the exhaust temperature reaches 948.50 K. The lambda values drop to 3.43 at IVC and 1.97 at EVO, indicating possible turbocharger limitations at high power levels. The engine achieves a maximum brake power output of 1215.75 kW.

The validation process involved comparing the simulated results from the W6L20 GT-Suite model with experimental in-cylinder pressure data obtained under 50% load conditions with the converted single-cylinder engine (SCE) which is denoted as W20 DF-SCE. This validation is critical to ensure the accuracy of the simulation before conducting an extensive parameter sweep.

Following the conversion of the SCE model from the reference W6L20 six-cylinder configuration to more accurately replicate the real engine, alignment was achieved by adjusting the intake pressure. Meanwhile, key parameters such as indicated mean effective pressure (IMEP), trapped mass, and fuel mass entering the cylinder were maintained constant to ensure realistic engine operating conditions. Figure 3 presents a comparison of the experimental data, the reference W6L20-2STC model, and SCE simulation results. The simulated pressure curves closely match the experimental data, confirming the models´ accuracy in representing combustion characteristics. The pressure was normalized relative to the experimental maximum pressure and total fuel energy, with peak pressure predictions exhibiting deviations of 1.93 bar and 1.89 bar.

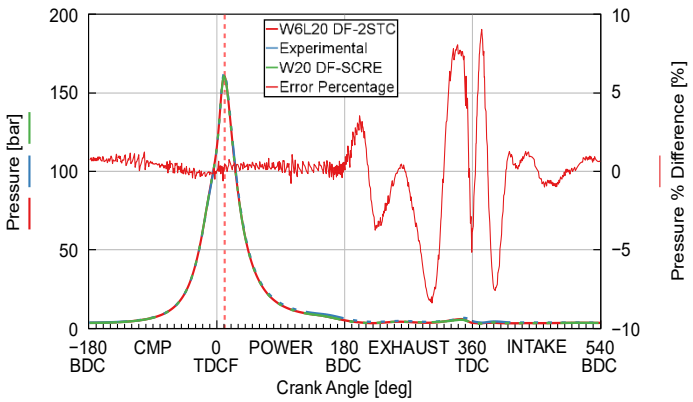

Figure 3: Comparison of experimental and simulated in-cylinder pressure curves for the W6L20-2STC and SCE models at 50% load conditions

The maximum in-cylinder pressures at approximately 11° crank angle were compared for the experimental data, W6L20 DF-2STC, and W20 DF-SCE models. The peak pressure values obtained were 162.94 bar, 161.01 bar, and 161.05 bar, respectively. These figures equate to simulated-to-experimental peak pressure accuracies of 98.81% for the W6L20-2STC model and 98.84% for the SCE model. These results underscore the models' high accuracy, marred only by a higher error near TDC, which was perhaps negligible since deterministic simulation was used.

The slightly elevated discrepancies observed during the intake and exhaust strokes in the single-cylinder model, relative to the full six-cylinder configuration, are primarily attributed to the absence of pulsating flow and transient pressure dynamics within the intake and exhaust manifolds. In a multi-cylinder engine, these unsteady flow

phenomena play a critical role in shaping cylinder filling and scavenging. When such effects are idealized or omitted in a single-cylinder model, a systematic deviation in predicted in-cylinder pressure can arise, particularly during exhaust strokes. This validation process confirms the SCE model's readiness for integration into the final six-cylinder closed-loop H-APC model for subsequent analysis.

3.1.2 Functional validation of the H-APC model

Figures 4 (a and b) depict the simulated pressure and temperature profiles within the W20 DF-SCE engine model, tested with two distinct gas mixtures: argon-oxygen (78% Ar + 22% O_2) and air (78% N_2 + 22% O_2). Both gas mixtures were evaluated under identical motoring conditions, with a constant in-cylinder flow rate of 214.25 g/s, and no fuel was injected during the experiment.

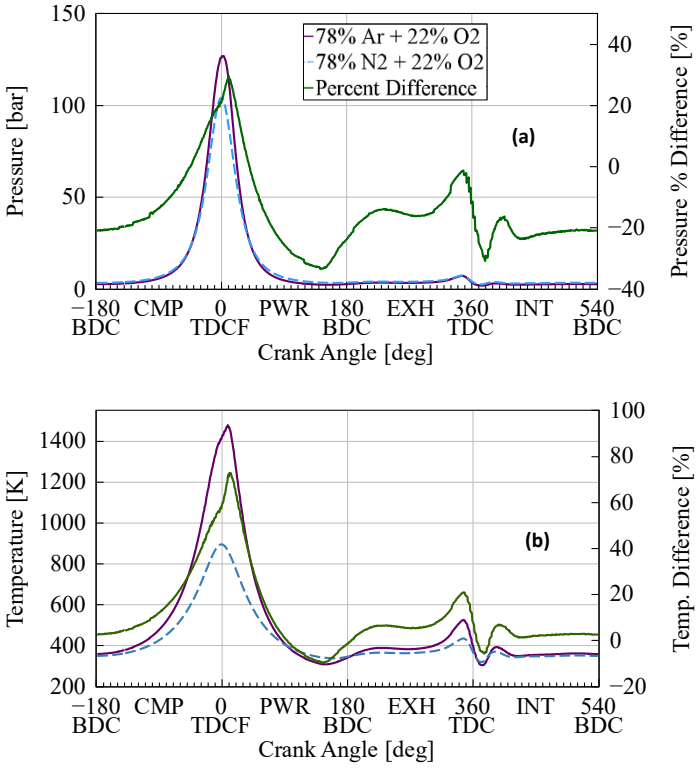

Figure 4: In-cylinder pressure and temperature profiles comparison for argon-oxygen and air mixtures in W20 DF-SCE engine: (a) pressure vs. crank angle, (b) temperature vs. crank angle at motored condition

Figure 4(a) illustrates the motored pressure as a function of crank angle, with both mixtures reaching peak pressure at top dead centre (TDC). The argon-oxygen mixture exhibits a maximum pressure of 127.06 bar, surpassing the 104 bar for the air mixture, indicating superior combustion efficiency. Pressure declines rapidly beyond TDC, and the fluctuations observed during the exhaust and intake strokes are clearly attributed to recompression due to negative valve overlap. Figure 4(b) presents the in-cylinder temperature profiles. The argon-oxygen mixture achieves a peak temperature of 1477 K, significantly exceeding the 895 K observed for the air mixture. This elevated temperature persists throughout the exhaust and intake phases, consistent with the imposed burn rate.

Simulation result showed that the use of argon as a working fluid significantly enhanced thermal efficiency of the reference engine due to its high specific heat ratio (γ), as theoretically demonstrated in recent research by Ahammed [10].. This increases pressure and temperature during adiabatic compression and expansion, following the relations $P \propto V^{-\gamma}$ and $T \propto V^{1-\gamma}$. Compared to air, which contains nitrogen with a lower γ, argon enables higher peak pressures and reduced heat loss owing to its inertness. Literature further indicates that hydrogen, when used with an argon-oxygen mixture, offers performance benefits but poses challenges such as high diffusivity, leakage risk, a wide flammability range (4–75%), low ignition energy, and an auto-ignition temperature ranged between 858 K to 953 K ± 8 K, depending on intake pressure, mixture composition and dilution ratio [24] [25]. These factors increase the likelihood of pre-ignition, knocking, and thermal loading, particularly under lean-burn conditions. They necessitate precise control of compression ratio and ignition timing, plus use of advanced sealing, high-temperature materials, and robust cooling systems [14].

3.1.3 Determining the design constraints for H-APC

Following a simulation sweep of the reference engine in Figure 2 and analysis of the resulting data, a closed-loop design constraint was defined, based on the maximum operating point of the engine. This constraint ensures that the new closed-loop system remains within the engine's operational limits, thereby preventing structural damage and performance degradation.

Under full-load operation, the design must comply with the critical limits outlined in Table 3 to achieve optimal power output, pressure and temperature control, and energy conversion efficiency. Table 2 lists the targeted design constraints at 75% load. It specifies the following parameters: a net efficiency of 60%; in-cylinder pressures between 230–250 bar; a maximum in-cylinder temperature of 3000 K; a power output of 1200 kW; and exhaust gas temperatures ranging from 950–1200 K.

Table 3: Overview of targeted engine design constraints at 75% load condition

Parameters	Design requirement
Net efficiency (%)	60
Maximum in-cylinder pressure (bar)	230 and 250
Maximum in-cylinder temperature (K)	3000
Power output (kW)	1200
Maximum exhaust gas temperature (EGT) (K)	950 and 1200

Achieving 60% net efficiency requires advancements in combustion chamber geometry, oxygen-fuel mixing, and heat recovery systems. The specified pressure and temperature limits necessitate the use of high-performance materials and thermal barrier coatings. Additionally, the exhaust gas temperature constraints demand effective cooling system design and advanced emissions control technologies to ensure efficient energy recovery and regulatory compliance. These parameters define the performance envelope required to develop a high-efficiency engine system capable of meeting stringent operational and environmental demands.

3.2 Determining optimum mixture composition for H-APC

3.2.1 Effect of argon/oxygen ratio

The study investigated the optimal argon-to-oxygen-to-fuel ratio for maximizing combustion efficiency in the H-APC W6L20 engine at 50%, 75%, and 100% loads in order to understand the effect of the Ar to O_2 ratio. The argon-to-oxygen ratio is adjusted by varying argon pressure, while hydrogen fuel mass and oxygen levels stabilize power output. Combustion parameters remain constant, with a fixed hydrogen-to-oxygen ratio of 1:8.

The tested argon-to-oxygen mixtures used 90% argon–10% oxygen; 88% argon–12% oxygen; 85% argon–15% oxygen; and 80% argon–20% oxygen. The condenser efficiency (95%), coolant temperature (345 K), and compression ratio (12.3:1) remain unchanged. Since the combustion burn rate was held constant across cases, the model may not capture potential combustion instability or slower kinetics with high argon dilution. In reality, very high argon fractions could lead to slower flame propagation, which would need advanced ignition or pre-chamber solutions [26]. The simulation results presented in Figure 5 assume those challenges are solved by control systems. This analysis assumes an effective argon recycling, but in practice, leakage or less-than-ideal separation would lower efficiency over time, which will be discussed in the last sweep of simulations.

At 50% load, reducing argon concentration from 90% to 80% lowers boost pressure from 2.65 bar to 1.87 bar, while net efficiency decreases from 55.59% to 50.70% and brake efficiency from 47.90% to 43.98%. Maximum in-cylinder pressure declines from 190.94 bar to 139.52 bar, while exhaust gas temperature rises from 817.88 K to 1062.40 K. Indicated and brake power remain stable at 690 kW and 604 kW, respectively.

Similarly, at 75% load, this reduction in argon concentration lowers boost pressure from 3.12 bar to 2.00 bar, necessitating an increase in fuel injection mass from 300 mg/c to 336 mg/c. Gross efficiency declines 58.5% to 51%; net efficiency declines from 56% to 49.32%; and brake efficiency drops from 50.11% to 44.85%. In-cylinder pressure falls from 238.59 bar to 168.60 bar, with peak temperature increasing from 2740.36 K to 2942.03 K. Exhaust and downpipe temperatures rise, indicating greater thermal losses.

At 100% load, this reduction in argon concentration reduces boost pressure from 3.93 bar to 2.21 bar, while fuel mass increases from 378.71 mg to 440.00 mg. Indicated efficiency declines from 58.04% to 49.09%, and brake efficiency decreases from 53.40% to 45.52%. Maximum in-cylinder pressure drops from 282.01 bar to 184.15 bar, while peak temperature rises from 2695.52 K to 3051.36 K. Exhaust gas temperature increases significantly, from 977.98 K to 1568.78 K., Indicated power remains at approximately 690 kW across all loads, while brake power fluctuates slightly around 604 kW.

At full-load conditions, boost pressure is significantly influenced by fuel mixture composition, which directly affects both volumetric efficiency and the effective compression ratio. A more reactive mixture (higher γ) enhances combustion kinetics, reducing heat retention and, consequently, the required boost pressure. In a mixture comprising 90% argon (Ar) and 10% oxygen (O_2), the high argon concentration acts as a thermal buffer, stabilizing combustion while necessitating higher boost pressure due to increased heat absorption during compression. In contrast, higher oxygen concentrations (15%-20%) accelerate combustion, reducing the required boost pressure. This aligns with the thermodynamic principle that compression work is inversely proportional to mixture reactivity, wherein more efficient combustion demands less compression.

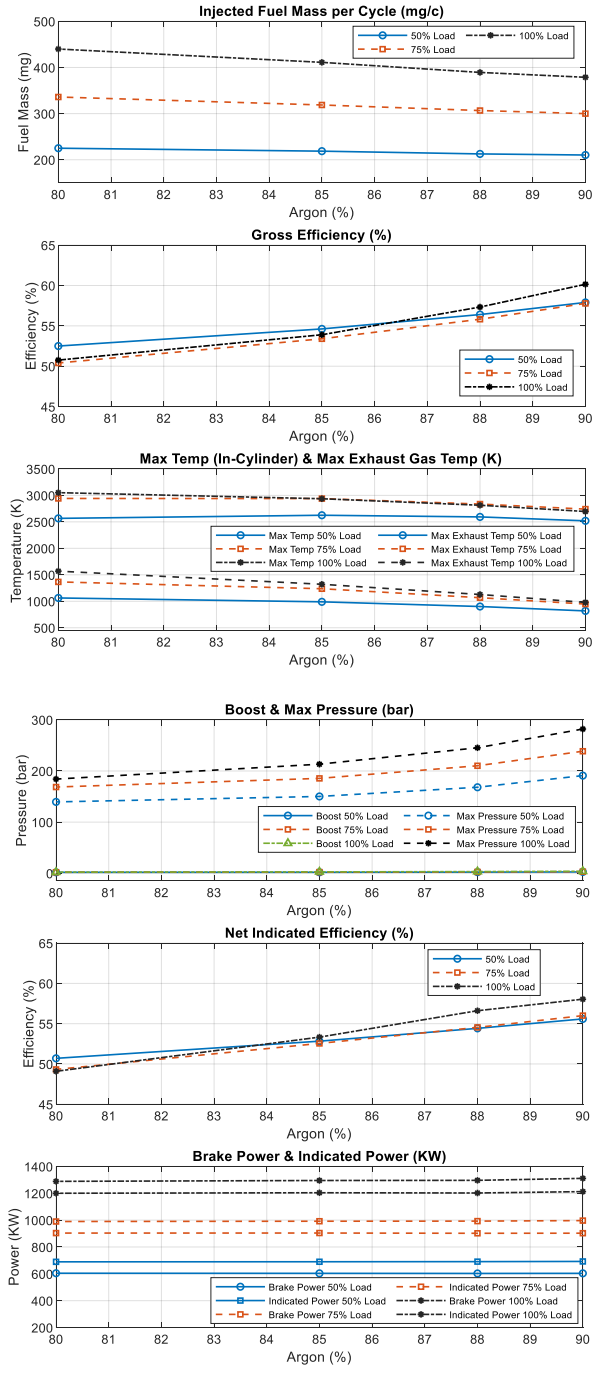

Figure 5: Performance metrics analysis of closed-loop H-APC at 50%, 75% and 100% load condition for different diluted mixture compositions

A reduction in argon concentration increases combustion temperatures while lowering in-cylinder pressure. This phenomenon results from elevated oxygen content, which increases fuel reactivity while diminishing argon's moderating effect. Additionally, a lower specific heat ratio at intake valve closure (IVC), due to decreased argon

content, exacerbates combustion temperature rise. Higher oxygen fractions lead to a slight reduction in both indicated mean effective Pressure (IMEP) and brake mean effective pressure (BMEP), because accelerated combustion lowers peak pressures, thereby reducing indicated efficiency. This decline stems from decreased thermal retention, impairing the engine's ability to convert heat into useful work.

Table 4 summarises the results from the simulated parametric sweep in terms of the engine design constraints, including maximum in-cylinder pressure (230 bar); temperature (3000 K); and efficiency (60%). It confirms that mixtures containing 90% Ar and 10% O_2, as well as 88% Ar and 12% O_2, satisfy these constraints. Conversely, a mixture of 80% Ar and 20% O_2 yields unacceptably low efficiency (49.90%) and surpasses thermal limits, increasing the risk of component failure. Excess oxygen elevates exhaust temperatures (1062 K) by enabling greater fuel consumption per cycle, leading to increased heat rejection and potential material stress. Despite potential cost advantages for the W6L20 engine, this mixture would necessitate extensive modifications, such as advanced thermal insulation and reinforced exhaust components, to mitigate thermal failure risks.

Table 4: Summary of the mixture composition sweep

Mixture Composition (Ar/O_2)	Max Pressure ≤ 230 bar	Max Temperature ≤ 3000 K	Efficiency ≥ 60%	Comments
90% / 10%	✅	✅	✅	Meets all design constraints
88% / 12%	✅	✅	✅	Meets all design constraints
80% / 20%	❌	❌	❌ (49.90%)	Fails: Low efficiency and exceeds thermal limits

Therefore, maintaining an argon concentration between 88% and 90% is recommended across all operational load conditions to optimize performance, ensure thermal stability, and enhance component durability.

3.2.2 Influence of alternative monatomic gases on H-APC performance

This simulation sweep evaluates the performance of the closed-loop H-APC W6L20 engine using pure argon, pure helium, and a 50%-50% argon-helium mixture. Figure 6 summarises the results. Simulations were conducted at a 75% reference load with 90% dilution and 10% oxygen, while maintaining a constant fuel injection of 300 mg/c result. Due to helium's low density, initial pressures were calibrated at 1.05 bar (argon); 23 bar (argon-helium); and 37.5 bar (helium) to prevent combustion instability and simulation failures. Boost pressure increased from 3.12 bar (argon) to 3.2 bar (helium).

Despite differences in initial pressure, IMEP720 (22.90 bar) and BMEP (20.50 bar) remained stable. Net efficiency exceeded 56%, while brake efficiency was highest for helium (50.28%). Maximum in-cylinder pressure peaked at 243.30 bar (helium), while in-cylinder temperature ranged from 2720.63 K (helium) to 2740.63 K (argon). The highest exhaust gas temperature was recorded for the argon-helium blend (950 K). Brake power ranged from 902.70 kW (argon) to 906 kW (helium), with indicated power from 996.49 kW to 1000 kW.

Monatomic gas combinations impact engine efficiency through density, thermal conductivity, and specific heat ratio. Pure argon, 1.4 times denser than nitrogen [10], results in lower initial and boost pressures, increasing mass flow, volumetric efficiency, and reducing pumping losses. Its density helps maintain high in-cylinder temperatures, improving flame propagation, reducing cooling losses, and enhancing energy conversion, leading to higher brake and indicated power output. An argon-helium mixture requires higher initial and boost pressures to offset helium's low density, increasing intake charge density and maintaining IMEP with slightly improved efficiency. However, helium's high thermal conductivity accelerates heat dissipation, lowering combustion temperatures and slightly reducing power output. Higher boost pressures also elevate mechanical load, increasing pumping losses. Pure helium demands very high initial pressures (up to 37.5 bar) to match intake mass flow, increasing frictional losses and mechanical inefficiency. Its high thermal conductivity further increases heat losses, reducing combustion temperatures and stability. Argon moderates flame speed, so its absence leads to combustion instability, localized high exhaust temperatures, and increased risk of knocking. These factors diminish net efficiency, despite the elevated pressures used to compensate for helium's low density.

The higher peak in-cylinder pressure for helium (~243 bar) compared to argon (~239 bar) is influenced by thermodynamic and transport properties. Helium's higher specific heat ratio ($\gamma \approx 1.66$ vs. argon's 1.67) results in steeper pressure rises during adiabatic compression, though the effect is minor. More significantly, helium's much higher speed of sound (~1007 m/s vs. ~319 m/s at 300 K) affects combustion dynamics by accelerating pressure wave propagation. This influences ignition delay, flame speed, and boundary-layer interactions, potentially leading to higher peak pressure. However, modeling artifacts in GT-Suite should be considered because simplifications, such as assuming perfect mixing, or neglecting local thermal diffusion, could introduce discrepancies. Accurate representation of helium's high diffusivity and thermal conductivity is essential, as these impact flame propagation and in-cylinder heat distribution. Experimental validation is needed to determine whether the observed differences in peak pressure are purely physical or influenced by model assumptions.

Noble gases such as neon and xenon offer potential advantages, given their high specific heat ratios. However, the practical application in ICEs, especially hydrogen-fuelled engines, is hindered by inherent limitations. Neon, due to its low density (0.90 kg/m³), necessitates high intake pressures and temperatures to ensure stable combustion. This reliance on external heating and the resulting heat losses significantly reduces system efficiency and complicates engine design. Xenon, with its low diffusivity and poor hydrogen mixing, and thus impedes combustion stability, leading to high peak temperatures, increased OH radical concentrations, and the potential for engine knocking. Its heavier molecular structure and suboptimal mixing characteristics necessitate high intake pressures (20 bar) and temperatures (1000 K), further exacerbating operational difficulties and inefficiencies [10].

The summary of the simulation sweep results has been tabulated in Table 5 for clearer illustration.

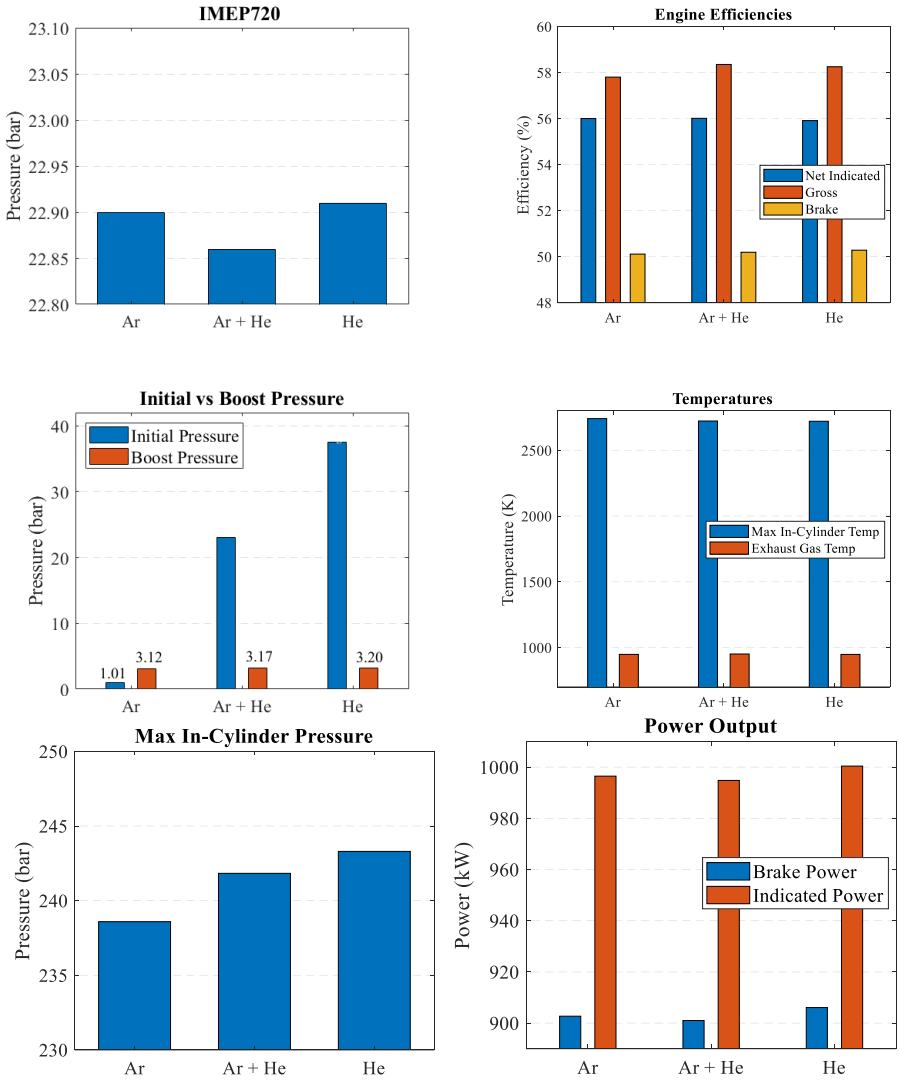

Figure 6: Performance analysis of various inert gas configurations in a six-cylinder W20 engine

Table 5: Summary of alternative monatomic gases analysis

Gas	Pmax ≤ 230 bar	Tmax. ≤ 3000 K	η ≥ 60%	Comments
Ar	✅	✅	✅	Meets all constraints; may need extra cooling due to high exhaust temperature.
He	❌	❌	❌	High pressure and low combustion temperatures reduce efficiency and stability.
50% Ar+ 50% He	✅	✅	✅	Balances stability and efficiency but require higher pressures.
Neon	❌	❌	❌	Low density causes instability and requires external heating (Simulation was not performed).
Xenon	❌	❌	❌	Poor mixing leads to instability and reduced efficiency (Simulation was not performed).

From a technical perspective, argon is identified as the optimal inert gas for the W6L20 H-APC engine, given its ability to meet all critical design specifications, including in-cylinder pressure, temperature limits, and efficiency thresholds. Compared to other inert gases, argon provides superior mixing rates, higher thermal buffering, and better control over flame propagation, all of which are essential for non-premixed combustion systems. Additionally, argon's higher density facilitates greater volumetric efficiency and lower pumping losses, making it more efficient and cost-effective for both emission reduction and standard engine applications. Its balance of thermal conductivity, specific heat ratio, and density makes it an ideal candidate for ensuring stable combustion, high energy conversion, and overall system efficiency. At this point argon as the most suitable inert gas for practical H-APC applications.

3.2.3 Influence of O_2 to H_2 ratio on combustion characteristics

Figure 7 shows the performance of the H-APC in a W6L20 engine through simulation sweep, focusing on the impact of the oxygen-to-fuel ratio (λ) on combustion efficiency and exhaust gas temperatures. The simulations are performed at a constant 75% load using a 90% argon and 10% oxygen mixture, with dynamic adjustment of injected hydrogen fuel mass for λ values of 0.85, 1.00, 1.20, and 1.40, while other combustion parameters remain fixed, based on the reference load.

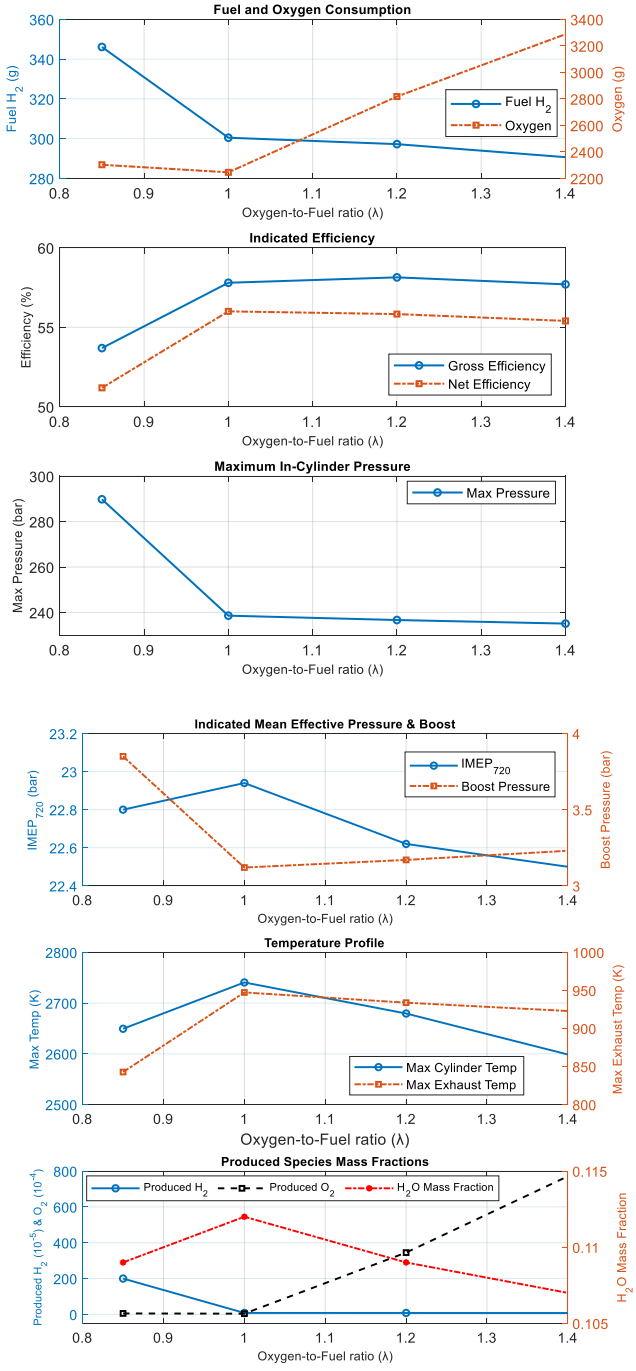

Figure 7: Impact of oxygen-to-fuel ratio on combustion dynamics and exhaust gas accumulation

At λ = 0.85 (rich mixture), fuel consumption is 346.11 mg, resulting in 51.19% efficiency, a peak pressure of 289.83 bar, and a combustion temperature of 2649 K. Exhaust temperature reaches 842.74 K, with increased H_2 indicating incomplete combustion and heat loss. At λ = 1.00 (stoichiometric), fuel consumption decreases to 300 mg, with efficiency improving to 56.00%. Peak pressure drops to 238.59 bar, and combustion temperature rises to 2740 K, while water mass fraction increases to 0.112, reflecting better combustion. For λ = 1.20 (lean mixture), fuel consumption falls to 292.22 mg and efficiency slightly decreases to 55.83%. Peak pressure is 236.67 bar, and combustion temperature is 2682 K. Exhaust temperature rises to 933.41 K. At λ = 1.40, fuel consumption is lowest at 290.65 mg, but efficiency declines to 55.40%. Peak pressure decreases to 235.10 bar, and temperature drops to 2598.66 K. Unburnt H_2 (7.71) and O_2 (771) increase, with exhaust temperature at 922.91 K.

This analysis demonstrates that the net indicated mean effective pressure (IMEP) remained constant across all conditions, ensuring stable power output, despite variations in the oxygen-to-fuel ratio. This stability was maintained by adjusting the injected fuel quantity. Indicated efficiency increased from 51.19% at λ = 0.85 to a peak of 56.00% at λ = 1.00, confirming the higher thermal efficiency of a stoichiometric mixture. However, as λ increased, maximum in-cylinder pressure and temperature and efficiency declined. The highest recorded pressure of 289.83 bar at λ = 0.85 indicates that richer mixtures intensify combustion, thereby increasing thermal stress. Exhaust gas temperature peaked at λ = 1.00, decreasing as the mixture became leaner. At λ = 1.40, an increase in oxygen-rich byproducts suggests incomplete combustion due to limited flame propagation and excess oxygen. The slight efficiency drops at λ=1.2 (lean) to λ=1.40 are partly due to increased heat loss. The mass fraction of water was greatest at stoichiometric conditions, where hydrogen and oxygen recombine most efficiently. Increasing λ improves combustion completeness but decreases efficiency beyond a certain threshold, highlighting trade-offs between efficiency, fuel economy, and emissions.

A comparative evaluation of different oxygen-to-fuel ratios highlights trade-offs between combustion efficiency, thermal stress, and byproduct formation within the design constraints of the W20 engine. Richer mixtures elevate in-cylinder pressure and temperature, increasing thermal stress while reducing byproduct formation. However, at high λ values, excess oxygen impairs combustion completeness. A stoichiometric mixture (λ = 1.00) is recommended, because it optimizes combustion efficiency while maintaining pressure and temperature within engine design limits. A slightly leaner mixture may be considered, as it significantly lowers exhaust gas temperature and so improves thermal management, but at the expense of a marginal reduction in efficiency.

3.3 Effect of compression ratio and exhaust gas pressure on combustion dynamics

3.3.1 Compression ratio effect

Figure 8 depicts how varying CR affects engine performance and combustion dynamics. The CR was swept from 6:1 to 12.3:1. Throughout the simulated investigation, the similar reference load and combustion parameters for 75% load used while consistent 300 mg fuel of H_2 per cycle were maintained. As CR increases from 6:1 to 12.3:1, boost pressure shifts slightly from 3.12 to 3.10 bar. IMEP and BMEP rise from 20.3 bar and 17.93 bar at CR 6:1 to 22.94 bar and

20.53 bar at CR 12.3:1, stabilizing at 22.90 bar and 20.50 bar at CR 11.90:1.

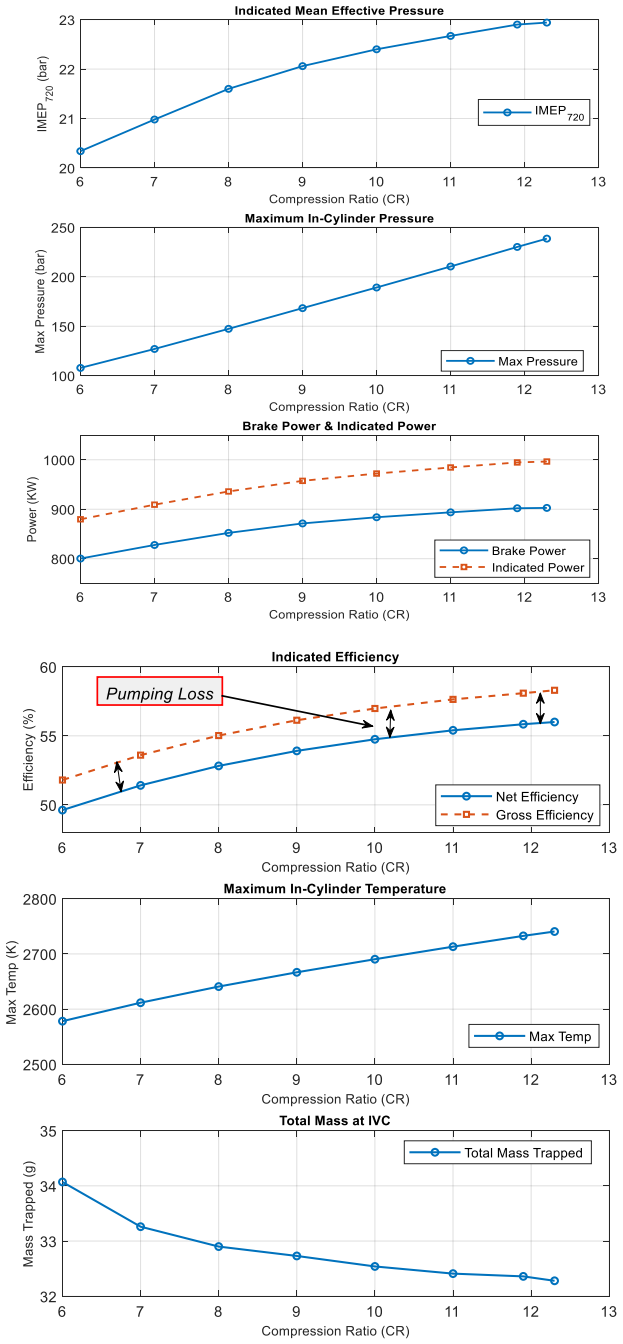

Figure 8: Impact of compression ratio variation on engine performance metrics

Efficiency improves with increasing CR, with indicated efficiency rising from 49.62% to 56.00%, and brake efficiency from 43.73% to 50.11%. Maximum cylinder pressure increases from 107.87 bar at CR 6:1 to 238.58 bar at CR 12.3:1, while in-cylinder temperature rises from 2578.21 K to 2740.60 K. Both pressure and temperature slightly decrease at CR 11.90:1, with negligible impact on efficiency. Brake power increases from 800.27 kW at CR 6:1 to 902.67 kW at CR 12.3:1, remaining constant at CR 11.90:1. The lambda value at intake valve closure rises from 3.43 to 3.81, and trapped mass decreases due to reduced clearance volume.

Results reveal that reducing the compression ratio leads to a decrease in boost pressure, indicated efficiency, maximum pressure, temperature, and brake power. The decrease in CR increases the volume at TDC, lowering the boost pressure requirement, while also exacerbating thermal losses and diminishing combustion efficiency. Applying the ideal gas law and adiabatic process equations shows that lower CR reduces the pressure-volume ratio, leading to lower peak combustion pressures and temperatures.

This results in a slower pressure rise, less energy release, and reduced overall efficiency. Brake power is directly impacted due to the declines in IMEP and thermal efficiency. Despite previous studies recommending CR 7:1-9:1, this research identifies CR 11.90:1 as optimal, achieving 900 KW at 75% load, with 230 bar and 3000 K peak conditions. Thus, CR 11.90:1 is recommended for further H-APC optimization in the W20 engine.

a) Auto-ignition analysis

The auto-ignition temperature is influenced by several factors, including in-cylinder temperature, pressure, and the presence of impurities. Studies by Chintala et al. have shown that hydrogen can auto-ignite at temperatures around 953 K ± 8 K in a compression ignition engine under dual-fuel mode, with the in-cylinder temperature being a critical factor for auto-ignition [24]. The auto-ignition characteristics of hydrogen for the W6L20 engine were analysed through simulations at varying CR specifically 6.0:1, 7.0:1, 8.0:1, 9.0:1, 10.0:1, 11.0:1, 11.9:1, and 12.3:1. The auto-ignition temperature for hydrogen was assumed to be 955 K to determine the corresponding crank angle where auto-ignition is achieved. Under the given conditions the Crank Angle for early Hydrogen Auto-Ignition (CA-H2 Auto ign) has been illustrated in Figure 9.

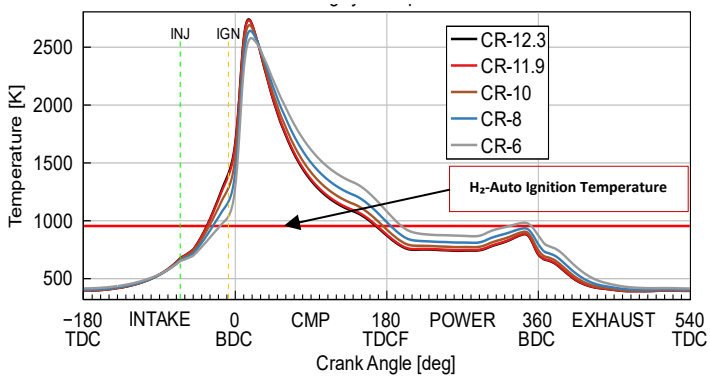

Figure 9: Analysis of in-cylinder temperature profiles across different compression ratios

The simulation results in Figure 9 demonstrated that increasing the compression ratio significantly advances the crank angle of hydrogen auto-ignition. This temperature's phasing-angle shows a notable shift as the compression ratio increases. Starting at a CR of 6.0:1, auto-ignition occurred at −22.87° crank angle after top dead center (CA ATDC), whereas at a CR of 12.3:1, it advanced to −33.86° CA ATDC.

Similarly, in Figure 10 early hydrogen auto-ignition (CA-H_2 Auto) is defined as the initial detectable combustion event, shifted from −11.09° CA ATDC at CR 6.0:1 to −27.02° CA ATDC at CR 12.3:1. Throughout these variations, the start of combustion (CA02), identified as the crank angle at which 2% of the fuel mass was burned, was maintained consistently at −6.94° CA ATDC to isolate the impact

of compression ratio on ignition phasing. This shift in combustion timing reflects the earlier onset of hydrogen combustion as the compression ratio increases. The advancement of the ignition timing indicates a more uncontrolled combustion process, which could affect engine performance and impact on undesirable thermal loading, although careful calibration is required to avoid knocking. Furthermore, increasing the compression ratio was found to enhance thermal efficiency. The net indicated efficiency improved from 49.62% at CR 6.0:1 to 56.00% at CR 12.3:1, while the gross indicated efficiency increased from 51.80% to 58.25% over the same range. This trend aligns with thermodynamic expectations, as higher compression ratios raise in-cylinder pressures and temperatures, facilitating earlier attainment of the auto-ignition threshold and enabling combustion initiation closer to optimal conditions.

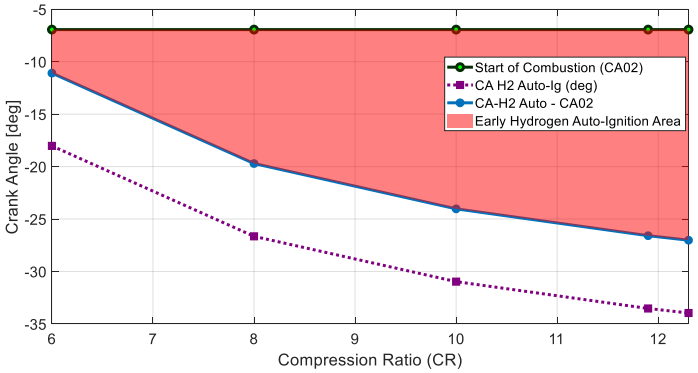

Figure 10: Variation of crank angle for early hydrogen auto-ignition with compression ratio, showing a decrease as the compression ratio increases, indicative of a shift towards more controlled combustion

The results derived from the simulation data have shown that, from a combustion dynamics perspective, the earlier ignition timing observed at higher CRs can be attributed to hydrogen's sensitivity to increased pressures and temperatures. Although earlier combustion improves thermal efficiency by enhancing expansion work and reducing heat losses, it also elevates the risk of knock and rapid pressure rise, potentially compromising engine durability. Consequently, advanced combustion control strategies, such as inert gas dilution, precise ignition timing management, and adaptive phasing control, are necessary to balance efficiency gains with operational stability.

It is important note that in these closed-loop H-APC simulations, auto-ignition phenomena were not explicitly modeled. Combustion was assumed to occur based on predefined timing, without accounting for spontaneous ignition events. The findings of this study indicate that at higher compression ratios, spontaneous hydrogen auto-ignition becomes a dominant factor, necessitating the integration of detailed ignition chemistry models in future simulations for more accurate predictions. Investigating the effects of compression ratios in auto ignition of H_2 through this system level simulation shows a clear correlation between the increasing compression ratio and both the earlier hydrogen auto-ignition and retarded combustion angles.

Increasing the compression ratio in hydrogen-fueled H-APC engines advances hydrogen auto-ignition and combustion phasing, thereby improving thermal efficiency. However, these advantages must be carefully balanced against the elevated knock risk and associated mechanical stresses. Future research should focus on developing robust combustion control techniques and thermal management strategies to maximize the benefits of hydrogen as a clean and efficient energy carrier in this advanced power cycle

b) Higher compression ratio trade-offs and design limits

Determining the optimal CR for the targeted engine design necessitates careful consideration of several key factors. First, maximum in-cylinder pressure thresholds of 230 bar and 250 bar were set for consideration, coupled with an upper temperature limit of 3000 K. Second, exhaust gas temperatures were set to be maintained between 950 K to 1200 K, ensuring thermal efficiency and mechanical integrity.

Figure 11 shows that increasing the CR produces proportional rises in both maximum in-cylinder pressure and temperature. They reach 230 bar and 2732.7 K respectively at CR 11.90:1; rising to 250 bar and 2750.94 K respectively at CR 12.85:1.

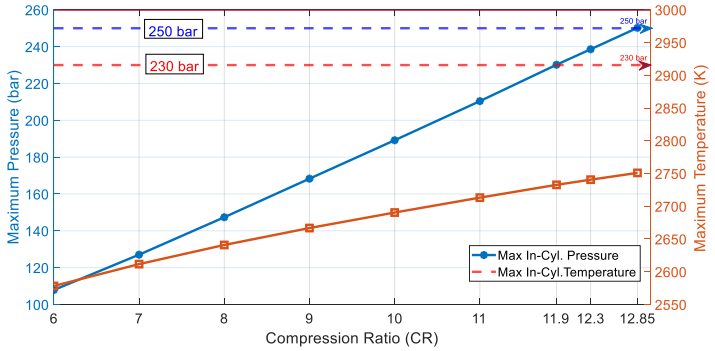

Figure 11: Effect of compression ratio on engine parameters, showing increased pressure and temperature

Higher CR improved efficiency, with indicated efficiency rising from 55.84% at a CR 11.9: 1 to 56.20% at a CR 12.85:1, while net IMEP remains stable. Brake power holds at 902–903 KW, and indicated power slightly increases from 994.61 KW to 998.23 KW. Exhaust temperature also goes upwards from 947.24 K to 951.70 K, ensuring thermal compliance.

Increasing the CR to 12.85:1 raises in-cylinder pressure to 250 bar, improving thermal efficiency but also intensifying mechanical stress on critical components such as pistons, connecting rods, and the cylinder head. This heightened load increases the risk of fatigue, wear, and long-term durability issues, necessitating a careful balance between efficiency gains and mechanical reliability. Moreover, higher CR amplifies knock susceptibility, potentially compromising performance and component integrity. Addressing these challenges requires advancements in combustion stability, knock resistance, and material durability to withstand elevated stresses. A strategic approach to CR selection must optimize efficiency while ensuring long-term reliability, minimizing maintenance demands, and preventing premature failure.

3.3.2 Exhaust backpressure analysis

The simulation sweep assesses the impact of exhaust back pressure on engine performance was conducted at 75% load, using a 90% argon–10% oxygen mixture and a fixed fuel injection rate of 300 mg/c. Four exhaust pressures before the condenser (3.23, 3.32, 4.02, and 4.26 bar) were analyzed. Figure 12 shows the results. The highest IMEP (22.90 bar) and net indicated efficiency (56.00%) were recorded at 3.23 bar. Peak in-cylinder temperature and pressure reached 2740.63 K and 238.59 bar, respectively. Indicated power was 996.49 KW. Exhaust and downpipe temperatures were 947.28 K and 858.63 K.

Increasing the backpressure to 3.32 bar slightly reduced IMEP to 22.75 bar. Efficiency fell marginally to 55.74%, lowering power to 977.91 KW. Raising backpressure again, to 4.02 bar, caused a further reduction in IMEP and efficiency to 21.79 bar and 53.11%, respectively. Power decreased to 914.66 KW. Peak pressure rose to 261.24 bar due to increased intake pressure after the ejector. When backpressure was raised to 4.26 bar, IMEP and efficiency reached their lowest values (21.71 bar and 53.05%), with power dropping to 907.92 KW. The findings underscore the detrimental effects of increased backpressure on efficiency, IMEP, and power.

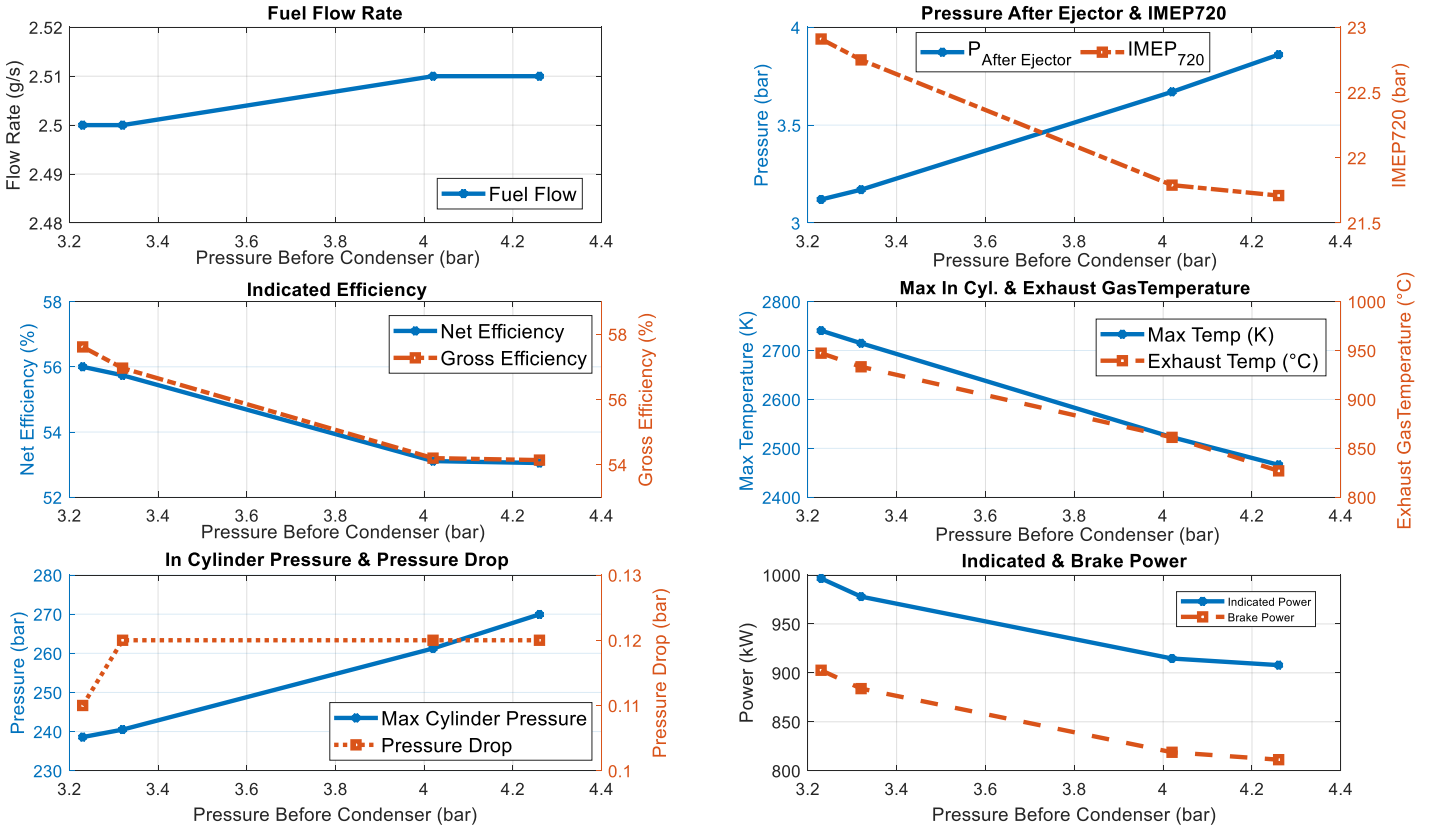

Figure 12: Impact of exhaust backpressure on combustion dynamics and efficiency, showing its effect on engine performance and overall efficiency

Elevated exhaust backpressure increases pumping losses, reducing IMEP and net power output. Argon's high specific heat capacity exacerbates heat retention, lowering the thermal gradients necessary for efficient combustion. Consequently, reduced exhaust temperatures indicate incomplete energy conversion, leading to lower indicated efficiency due to slower flame propagation and incomplete combustion. Additionally, argon´s inert nature and reduced oxygen availability limit mixture reactivity, while increased residual gas content reduces volumetric efficiency by displacing fresh reactants. Continuous argon recirculation in closed-loop systems compounds thermal load, causing further deterioration in efficiency.

Higher backpressure disrupts exhaust scavenging, elevating in-cylinder temperatures and increasing residual gas content, negatively affecting combustion stability. Optimization of valve timing, enhanced exhaust geometry, and turbocharger control are necessary [10]. A baseline exhaust pressure of 3.23 bar is recommended for optimal efficiency, while 3.32 bar may be viable with improved exhaust design, such as larger diameter pipes or multiple runners. Variable valve timing (VVT) can further optimize scavenging under fluctuating conditions. A key finding from this simulation sweep is that increased boost pressure, which also increases backpressure, lowers exhaust gas temperatures, highlighting a crucial area for further investigation in exhaust gas management to enhance engine performance.

3.4 Impact of fuel impurities on combustion and efficiency

This study investigated the impact of impurities in industrial-grade hydrogen on engine performance: previous simulations considered only pure hydrogen and oxygen. In practice, hydrogen typically contains trace gases such as N_2, CO, and CO_2, which lower the specific heat ratio and progressively degrade thermodynamic efficiency. Additionally, impurities originating from lubricating oil contribute to particulate formation. The simulation setup the model assumed a working fluid comprising 90% argon and 10% oxygen, and a fuel mixture of 98% hydrogen and 2% nitrogen, supplied through an H_2 controller unit. It was operated at 75% load. The simulation was conducted over time to examine the extent of impurities in hydrogen fuel influence engine performance and the rate at which they reduce efficiency. Furthermore, impurity build-up was simulated by incrementally increasing 2% N_2 in the recycled argon during each cycle, as it was neither separated nor removed, leading to continuous recirculation within the system. Figure 13 presents engine performance as hydrogen is progressively diluted with 2% N_2 mixture. Initially, with pure hydrogen (0 minutes), the engine achieves peak performance, with an IMEP of 22.90 bar, thermal or gross efficiency of 57.78%, and indicated power of 996.49 kW. The peak pressure and

temperature are recorded at 238.59 bar and 2740.36 K, respectively, with a brake power of 902.70 kW.

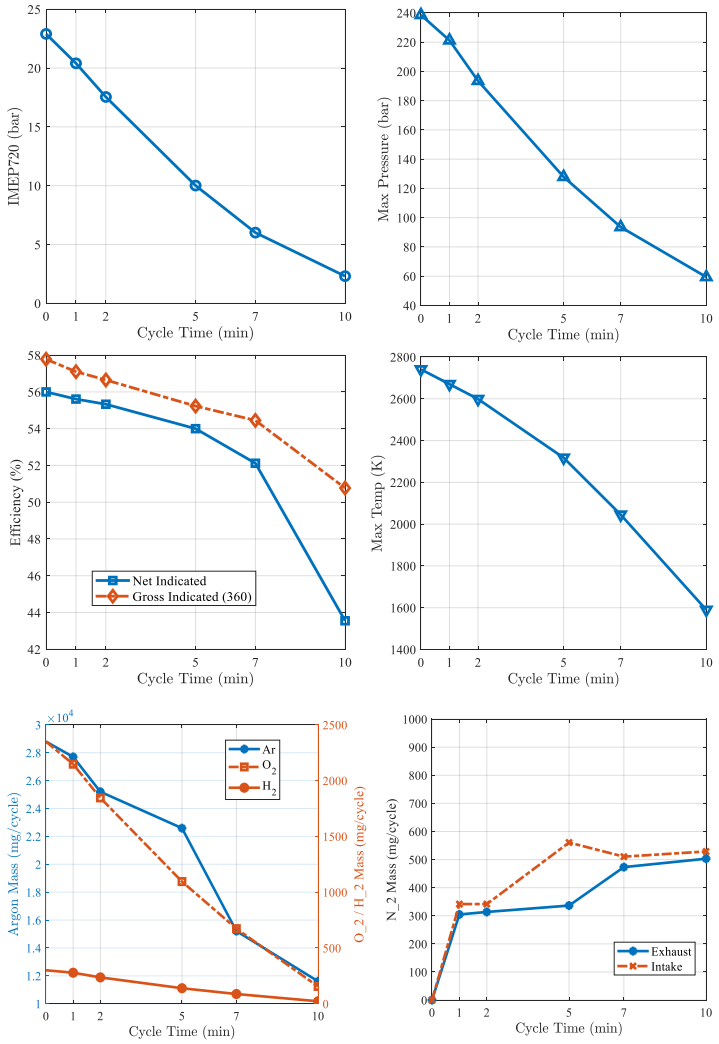

Figure 13: Effect of hydrogen fuel impurities on engine performance, illustrating their impact on combustion efficiency and overall system performance

Engine performance deteriorates as hydrogen is progressively diluted. After 10 minutes, the IMEP drops significantly to 2.31 bar, while indicated efficiency falls to 43.55% and gross efficiency decreases to 50.77%. Maximum pressure and temperature are reduced to 59.42 bar and 1589.78 K, respectively. Correspondingly, brake power decreases to 24.58 kW, and indicated power drops to 98.70 kW. The fraction of nitrogen (N_2) in both intake and exhaust increases with time, reaching 0.039 and 0.041 after 10 minutes, compared to zero for pure hydrogen.

The mass of hydrogen and oxygen decreased from 2,350 to 155 mg/cycle and 300 to 22 mg/cycle, respectively, while the mass of argon decreased from 28,800 to 11,610 mg/cycle as cycle time increased. These results show that the concentration of other impurities in the gas mixture has been steadily declining over time. As a result of improved nitrogen conversion, nitrogen species production increased significantly at the same time. Exhaust-side Prod-n2-Species increased from 0 to 503.10 mg/cycle, while intake-side Prod-n2-Species mass increased from 0 to 528.90 mg/cycle. The thermodynamic behavior changes as the specific heat ratio drops from ~1.60 to 1.48. The substantial detrimental effects of impurities on engine performance and efficiency were demonstrated after ten minutes, when the indicated efficiency fell below 50% and fuel injection approached zero.

The simulation data clearly demonstrates the significant impact of hydrogen fuel impurities on the performance and thermodynamics of the simulated W6L20 engine. A notable reduction in the indicated mean effective pressure (IMEP) was observed, primarily due to the alteration of the working fluid mixture, which consists of argon and oxygen. This mixture is regulated by the specific output and injection controller designed to maintain the optimal oxygen-to-fuel ratio. However, the injection controller exhibited unexpected behavior due to the presence of nitrogen (N_2) impurities. Although the intake system detected the additional nitrogen, the controller was unable to adjust for it, leading to the accumulation of nitrogen in the closed-cycle argon recirculation system.

The accumulation of nitrogen significantly disrupted the intended composition of the working fluid, particularly the oxygen-to-fuel and argon ratios, resulting in substantial performance degradation. Specifically, nitrogen impurities reduced the specific heat ratio from 1.58 for pure hydrogen to 1.48, which lowered both combustion pressures and temperatures. This reduction in specific heat led to a decrease in engine efficiency, as reflected in the progressive decline of IMEP and overall thermal efficiency over time. After approximately 10 minutes of operation, engine performance was noticeably impaired, marked by a reduction in maximum in-cylinder pressure and temperature, which ultimately compromised combustion stability.

Furthermore, the accumulation of nitrogen impurities increased pumping losses, requiring more energy to expel exhaust gases containing non-combustible nitrogen. This inefficiency led to a widening gap between gross and net engine efficiency, exacerbating the overall degradation of engine performance. A critical limitation of the controller is its inability to monitor the impurity accumulation rate within the closed-cycle argon recirculation loop, which only expels condensed H_2O through the condenser unit. The failure to detect and adjust for the rising impurity concentration significantly contributed to the observed deterioration in engine performance over time. Low impurity levels (e.g., 2%) allow extended operation, but higher impurity concentrations necessitate frequent intervention to avoid further performance loss. Effective purification methods are crucial to mitigate the adverse effects of impurities. Gas-phase flash-off and in-cycle gas separators can remove volatile impurities and selectively separate non-combustible gases [27], [28]. These strategies preserve fuel purity, optimize combustion, and ensure sustained engine performance, thus enhancing efficiency and prolonging the lifespan of hydrogen-fueled engines such as the W20 engine.

3.5 Energy losses analysis across the engine cycle

The simulation analysis identified the optimal argon-to-oxygen mixture for the closed-loop H-APC as 90% argon and 10% oxygen. A CR of 11.90:1 was found to maximize engine efficiency. Stoichiometric mixtures ($\lambda = 1$) with an exhaust back pressure of 3.23 bar after the condenser improved combustion performance without exceeding thermal load limits. This cycle demonstrated higher performance gains than the traditional Otto cycle dual-fuel engine, but significant energy losses were observed. The Sankey diagram in Figure 14 provides insight into the energy distribution and loss mechanisms within the closed-loop hydrogen-argon cycle. The results are based on engine performance measurement in GT-Suite analysis and are affected by the simulation accuracy at the time of measurement. Cylinder pressure measurements and exhaust temperature and pressure

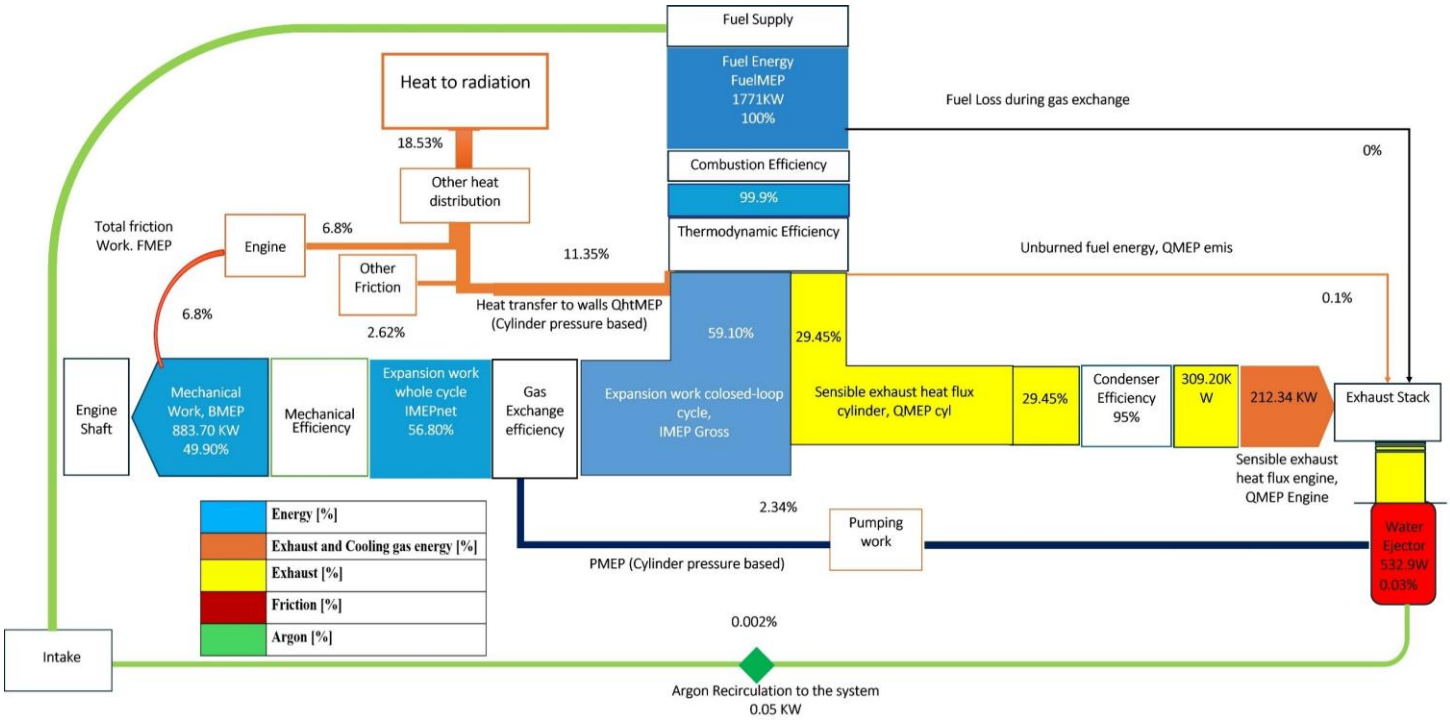

Figure 14 : Sankey diagram illustrating the energy flow within the closed-loop H-APC system, depicting energy inputs, conversions, and losses across key components of the cycle based on GT-Suite simulation

measurements have the largest uncertainties, due to the non-predictive combustion model used for the dual-fuel case.

Of the total 1,771 kW fuel energy input, 49.9% (883.7 kW) is effectively converted into mechanical work. The remaining energy is lost through thermal dissipation, friction, and pumping inefficiencies, all of which impact overall efficiency. Exhaust heat losses account for a substantial portion of these inefficiencies, with 29.45% of the input energy released as sensible heat flux, even with a 95% condenser efficiency. Additional losses include 309.2 kW from the condenser and 212.34 kW from the exhaust stack, emphasizing the need for thermal optimization. Frictional losses contribute 6.8% of the total energy loss, with engine and other mechanical friction making up 2.62%. Pumping losses, measured at 2.34%, impose further constraints on performance. The expansion process (IMEP_net: 56.8%) highlights efficient combustion energy utilization, while gas exchange dynamics significantly influence overall engine performance. Furthermore, auxiliary components such as the 532.9 W water ejector and the 0.05 kW argon recirculation system introduce minor parasitic losses.

Despite the system's relatively high efficiency, energy dissipation remains a challenge. Improving heat recovery, minimizing mechanical friction, and optimizing gas exchange are critical steps toward enhancing performance. Addressing these inefficiencies is essential for advancing closed-loop, hydrogen-argon cycle technology.

4 Conclusions and Outlook

This study presents, for the first time, a performance evaluation of a large-bore, medium-speed engine adopting the principles of Argon Power Cycle. By adapting a 1D-model of a prototype Wärtsilä 6L20 engine (bore 200 mm, stroke 280 mm) with an argon recovery loop, dedicated H_2/O_2 injectors, and a condenser-based water separator, the work brings forward following conclusions:

(i) Argon was identified as the most effective monoatomic gas for the H-APC, due to its favorable physical properties and compatibility with high-performance operation. Although helium provides higher thermal conductivity and specific heat capacity, its low density and molecular weight limit its capacity for power generation. A mixture of 90% argon and 10% oxygen offers the optimal balance between power output, thermal efficiency, and system durability.

(ii) A stoichiometric or slightly lean oxygen–fuel equivalence ratio (λ=1 to 1.2) was found to balance efficient and complete combustion maintaining accumulation of unburnt gas while maintaining exhaust gas temperatures within admissible limits. This balance enhances thermal efficiency and power output without causing excessive thermal stress or damage to engine components, leading to targeted performance and durability.

(iii) In the given configuration, peak indicated gross efficiency can reach 59.10% at 75% load while respecting the feasible limits of mechanical and thermal loading. Although packaging and pumping losses reduced net efficiency to 56.90%, the cycle still bettered the efficiency of conventional dual-fuel engines by a margin of roughly 10 percentage points.

(iv) An optimized compression ratio of 11.90 was found to maintain in-cylinder pressures under 230 bar, exhaust temperatures below 950 K, and combustion temperatures near 3000 K. This requires an argon fraction of 88–90% and a 10–12% oxygen fraction—significantly higher than what small-engine studies had suggested.

(v) A compression ratio of 11.90 provided robust mechanical margins and performance (peak pressure ~230 bar) while achieving ~996 kW of indicated power.

(vi) Excess exhaust backpressure hindered scavenging efficiency and forced incomplete energy recovery and increased pumping losses. Hydraulic Valve Timing (HVT)/VVT can improve scavenging by optimizing valve events, while Miller timing could reduce pumping losses by shortening the effective compression stroke. Together, these strategies restore energy balance and maintain optimal engine performance.

(vii) Even 2% of impurities in the hydrogen fuel caused efficiency to degrade by ~seven percentage points in just 10 minutes, primarily due to nitrogen (N_2) buildup in the closed cycle required further investigation on other trace gases build up. The excess N_2, a non-reactive gas, reduced the specific heat ratio (1.60 to 1.48) of the working fluid by 8%, significantly lowering thermal efficiency. This highlights the critical need for high-purity reactants and advanced separation techniques, such as gas-phase flash-off and in-cycle gas separators to remove inert gases and maintain optimal engine performance.

Collectively, these findings bridge the gap between single-cylinder H-APC research and full-scale peaking-power applications, highlighting the design trade-offs necessary for real-world deployments. They further emphasize that effective management of inert gas composition, oxygen levels, and fuel quality is critical to sustaining the cycle's efficiency and near-zero emissions over extended operation.

Study limitations and outlook on future work

Aside from providing initial design constraints for the Argon-Power-Cycle concept on Wartsila engine platform, this study establishes a model-based rapid-prototyping framework for rapid-prototyping of the concept. The framework at its current form exhibits some limitations. To this end, relevant improvement points from the perspective of model fidelity and predictivity include:

(i) Development of predictive phenomenological model for hydrogen/oxygen combustion in argon atmosphere. According to the present study, a feasible route for APC, relies on hydrogen compression-ignition, with combustion progress controlled by diffusion jet of either high-pressure injected hydrogen or oxygen. The auto-ignition phenomena is further entangled by the cross-influence of hot-source and lubricating oil induced pre-ignition that needs to be taken into account in predictive simulation.

(ii) Lack of comprehensive heat flux-measurements in argon atmosphere limits the accuracy of engine heat transfer correlations, limiting the accuracy of energy balance analysis and preventing implementing predictive wall thermal solvers for detail thermal loading studies in APC.

(iii) Implementing real condenser characteristics and exploring more advanced APC layouts, including turbo compounding.

The above drawbacks are currently being resolved in the scope of the iHAPC project [22]. To this end Optical Spray-Combustion Chamber (OSCC) and Rapid Compression Expansion Machine (RCEM) tests, feed detail 3D-CFD models of mixture formation, ignition and combustion, considering fuel-oil interaction and detail heat-flux calculations. Similar tests focus on developing bespoken condenser and turbocharging systems for APC. The high-fidelity models, after reduction, will be re-integrated into the current 1D-framework, allowing for expanding the scope of the present study into the following directions:

- Multi-parameter optimization of APC configuration under constraints of real combustion instability and mixture/flow condition-dependent water/impurity accumulation
- Developing control strategies for mitigating pre-ignition and excessive thermal loading in engine components.
- Expending the scope of 1D-simulations to system-level integration with power generation, Hydrogen/Oxygen production and storage.

The above model-based development targets ultimately support building the up-scaled APC technology demonstrator, targeting 60% efficiency at 150kW output power per-cylinder.

5 References

[1] I. Energy Agency, "Net Zero by 2050 - A Roadmap for the Global Energy Sector," 2024. [Online]. Available: www.iea.org/t&c/

[2] I. Renewable Energy Agency, *TRANSFORMING THE ENERGY SYSTEM-AND HOLDING THE LINE ON RISING GLOBAL TEMPERATURES 2*. 2019. [Online]. Available: www.irena.org

[3] I. Energy Agency, "Net Zero Roadmap: A Global Pathway to Keep the 1.5 °C Goal in Reach - 2023 Update," 2023. [Online]. Available: www.iea.org/t&c/

[4] S. Niemi *et al.*, "Performance and emissions of a medium-speed engine driven with sustainable options of liquid fuels Performance and emissions of a medium-speed engine driven with sustainable options of liquid fuels," 2020. [Online]. Available: https://www.sae.org/publications/technical-papers/content/2020-01-

[5] T. Fang and R. Lahdelma, "Optimization of combined heat and power production with heat storage based on sliding time window method," *Appl Energy*, vol. 162, pp. 723–732, Jan. 2016, doi: 10.1016/j.apenergy.2015.10.135.

[6] R. W. Dibble, M. Sierra Aznar, B. S. Timothy, and C. Jyh-Yuan, "RECIRCULATING NOBLE GAS INTERNAL COMBUSTION POWER CYCLE," 2015.

[7] S. Sebastian, S. Wijewardane, and S. Srinivasan, "Recent advances in hydrogen production, storage, and fuel cell Technologies with an emphasis on inventions, innovations, and commercialization," *Solar Compass*, vol. 8, p. 100065, Dec. 2023, doi: 10.1016/j.solcom.2023.100065.

[8] M. M. Kabir, M. M. Akter, Z. Huang, L. Tijing, and H. K. Shon, "Hydrogen production from water industries for a circular economy," May 15, 2023, *Elsevier B.V.* doi: 10.1016/j.desal.2023.116448.

[9] C. Wang, S. Jin, J. Deng, and L. Li, “An Innovative Argon/Miller Power Cycle for Internal Combustion Engine: Thermodynamic Analysis of its Efficiency and Power Density,” *Automotive Innovation*, vol. 6, no. 1, pp. 76–88, Feb. 2023, doi: 10.1007/s42154-022-00208-x.

[10] S. Ahammed, “Hydrogen-Argon Power Cycle (HAPC) on a Wartsila medium-speed engine: an Investigation using 1D-Simulation,” 2025. Accessed: Feb. 24, 2025. [Online]. Available: https://urn.fi/URN:NBN:fi-fe202501051357

[11] J. Kim, R. Scarcelli, G. Beardsell, T. Strickland, C. Nilsen, and M. Sierra Aznar, “Modeling Pre-Chamber Assisted Efficient Combustion in an Argon Power Cycle Engine,” in *SAE Technical Papers*, SAE International, Apr. 2024. doi: 10.4271/2024-01-2690.

[12] K. Xie, J. Deng, S. Jin, and L. Li, “Numerical Study on Flammability Limit and Performance of Compression-Ignition Argon Power Cycle Engine with Fuel of Hydrogen,” in *SAE Technical Papers*, SAE International, Apr. 2021. doi: 10.4271/2021-01-0391.

[13] Q. Zhang, Z. Zuo, and J. Liu, “Failure analysis of a diesel engine cylinder head based on finite element method,” *Eng Fail Anal*, vol. 34, pp. 51–58, Dec. 2013, doi: 10.1016/j.engfailanal.2013.07.023.

[14] S. Shi, Y. Tomomatsu, B. Chaturvedi, M. Sierra Aznar, and J. Y. Chen, “Engine efficiency enhancement and operation range extension by argon power cycle using natural gas,” *Appl Energy*, vol. 281, Jan. 2021, doi: 10.1016/j.apenergy.2020.116109.

[15] N. J. Killingsworth, V. H. Rapp, D. L. Flowers, S. M. Aceves, J. Y. Chen, and R. Dibble, “Increased efficiency in SI engine with air replaced by oxygen in argon mixture,” *Proceedings of the Combustion Institute*, vol. 33, no. 2, pp. 3141–3149, 2011, doi: 10.1016/j.proci.2010.07.035.

[16] K. Rentaro, K. Akira, K. Eiichi, and S. Daisaku, “Study of High Efficiency Zero-Emission Argon Circulated Hydrogen Engine,” 2010.

[17] L. Xinyu, S. Ales, Y. Ho Lung, and H. Evatt, “Comparison of hydrogen port injection and direct injection (DI) in a single-cylinder dual-fuel diesel engine,” 2020.

[18] H. S. Van Den Brink, “Where innovation starts Exploring injection strategies for the Argon Power Cycle in CONVERGE CFD Where innovation starts Exploring injection strategies for the Argon Power Cycle,” 2022. [Online]. Available: www.tue.nl

[19] M. Sierra Aznar, “Numerical and experimental investigation of the Argon Power Cycle for power generation efficiency improvement and emissions reduction,” 2018.

[20] R. W. Dibble, M. Sierra Aznar, T. B. Sennott, and J.-Y. Chen, “RECIRCULATING NOBLE GAS INTERNAL COMBUSTION POWER CYCLE,” 2017.

[21] M. Sierra Aznar, “Ultra-Efficient CHP with High Power/Heat Ratio Using a Novel Argon Power Cycle| IEDO,” 2023.

[22] University of Vaasa, “Integrated Hydrogen-Argon Power Cycle (iHAPC).” Accessed: Apr. 11, 2025. [Online]. Available: https://sites.uwasa.fi/ihapc/

[23] Wärtsilä, “Wärtsilä 20 Product Guide,” 2020.

[24] V. Chintala and K. A. Subramanian, “Experimental investigation of autoignition of hydrogen-air charge in a compression ignition engine under dual-fuel mode,” *Energy*, vol. 138, pp. 197–209, 2017, doi: 10.1016/j.energy.2017.07.068.

[25] A. L. Sánchez and F. A. Williams, “Recent advances in understanding of flammability characteristics of hydrogen,” 2014, *Elsevier Ltd*. doi: 10.1016/j.pecs.2013.10.002.

[26] S. Jin, B. Shu, X. He, R. Fernandes, and L. Li, “A study on autoignition characteristics of H2-O2 mixtures with diluents of Ar/N2 in rapid compression machine for argon power cycle engines,” *Fuel*, vol. 303, Nov. 2021, doi: 10.1016/j.fuel.2021.121291.

[27] J. Senda, Y. Wada, D. Kawano, and H. Fujimoto, “Improvement of combustion and emissions in diesel engines by means of enhanced mixture formation based on flash boiling of mixed fuel,” *International Journal of Engine Research*, vol. 9, no. 1, pp. 15–27, 2008, doi: 10.1243/14680874JER02007.

[28] E. Randolph, Graham Conway, Jason Herrera, Terrence Alger, Nishant Thakral, and Christopher Chadwell, “A Gas Separation Membrane Highly Selective to CO2 in the Exhaust of Internal Combustion Engines,” *2019 JSAE/SAE Powertrains, Fuels and Lubricants*, Dec. 2019.

Contact Information

Sajid Ahammed

Doctoral Researcher

University of Vaasa, School of Technology and Innovations,
Efficient Powertrain Solutions (EPS)

Wolffintie 32, 65200 Vaasa

Email: sajid.ahammed@uwasa.fi tel. +358 29 449 8597

Acknowledgments

This research was conducted as part of the Integrated Hydrogen–Argon Power Cycle (iHAPC) project, co-funded by Business Finland (ref. 10309/31/2023). The authors wish to acknowledge Mr. Aneesh Vasudev and Mr. Amir Soleimani (Efficient Powertrain Solutions) for their valuable support in developing and validating the simulation model.

Definitions/abbreviations

APC	argon power cycle
Ar	argon
BDC	bottom dead center
BMEP	brake mean effective pressure
CA	crank angle
CR	compression ratio
DF	dual fuel
DI	direct injection
EVO	exhaust valve opens
EGT	exhaust gas temperature
GTP	GT Power
H_2	hydrogen
H-APC	hydrogen-argon power cycle
He	helium
ICEs	internal combustion engines
iHAPC	Integrated Hydrogen-Argon Power Cycle project
IEA	International Energy Agency
IMEP	indicated mean effective pressure
IRENA	International Renewable Energy Agency
LHV	lower heating value
MDO	marine diesel oil
MFB	mass fraction burned
MFR	mass flow rates
NO_x	nitrogen oxide
PFI	port fuel injection
PM	particulate matter
RCEM	rapid compression expansion machine
SACI	spark-assisted compression ignition
SCE	single cylinder engine
SI	spark ignition
SL	laminar flame speed
TDC	top dead center
TDCF	top dead center firing
TPA	three-pressure analysis
VVT	variable valve timing
W6L20-2STC	Wärtsilä six-cylinder, two-stage turbocharged engine
λ	oxygen-to-fuel ratio
γ	specific heat ratio

Appendix 1

In the closed-loop system, efficiency is determined based on the indicated efficiency of the closed portion of the cycle, as derived from power analysis conducted within the GT-Suite model and post-processed using GT-Post. The reported efficiency of 59.10% specifically refers to the indicated efficiency, considering only the closed portion of the cycle and excluding any losses associated with external or open-loop systems. Since the system operates in a closed-loop configuration, there is no exhaust pipe, and therefore, exhaust losses are not relevant to the efficiency calculation.

Regarding the argon loop, the calculation of net efficiency incorporates the work required for pumping argon. This energy expenditure is included in the overall energy balance of the closed-loop system. Losses associated with pumping are reflected in the net efficiency value and are accounted for in the GT-Suite simulation, integrated into the total energy input/output calculations. These losses are not treated as separate exhaust losses, as the system does not rely on an open exhaust.